cmgh
CELLULAR AND MOLECULAR GASTROENTEROLOGY AND HEPATOLOGY

ORIGINAL RESEARCH

A New Model of Gastric Pre-neoplasia Induced by Aberrant ADAR1-mediated Double-stranded RNA Signaling

Angela M. Halstead,[1] Chinye Nwokolo,[1] Stella Hoft,[2] Jinsheng Yu,[3] Lifei Zhu,[4] Brendan Tuley,[1] Nancy Vargas,[1] RuiRui Liu,[1] Francisco Ramirez Victorino,[1] Simrin Phatak,[5] Wandy Beatty,[6] Chun-Kan Chen,[7] Richard DiPaolo,[2] Paul Cliften,[3] Tarin M. Bigley,[4] and José B. Sáenz[1,8]

[1]Division of Gastroenterology, Department of Medicine, Washington University in St. Louis School of Medicine, St Louis, Missouri; [2]Department of Molecular Microbiology and Immunology, St Louis University School of Medicine, St Louis, Missouri; [3]Department of Genetics, Washington University in St Louis School of Medicine, St Louis, Missouri; [4]Division of Pediatric Rheumatology, Department of Pediatrics, Washington University in St Louis School of Medicine, St Louis, Missouri; [5]University of Missouri-Kansas City School of Medicine, Kansas City, Missouri; [6]Department of Molecular Microbiology, Washington University in St Louis School of Medicine, St Louis, Missouri; [7]Department of Cell Biology and Physiology, Washington University in St Louis School of Medicine, St Louis, Missouri; and [8]Department of Molecular Cell Biology, Washington University in St Louis School of Medicine, St Louis, Missouri

ADAR1-mediated double-stranded RNA (dsRNA) signaling in gastric pre-neoplasia

Methods

- Genetic mouse model of gastric parietal cell-specific deletion of *Adar1* (*Adar1*$^{\Delta PC}$).
- Histologic, transcriptional, molecular, and flow cytometric characterization of age-matched control and *Adar1*$^{\Delta PC}$ mice.
- Source of gastric epithelial dsRNA determined by dsRIP-seq and by immuno-electron microscopy.

***Adar1*$^{\Delta PC}$ mice develop gastric pre-neoplasia dependent on type I and type III interferon signaling.**

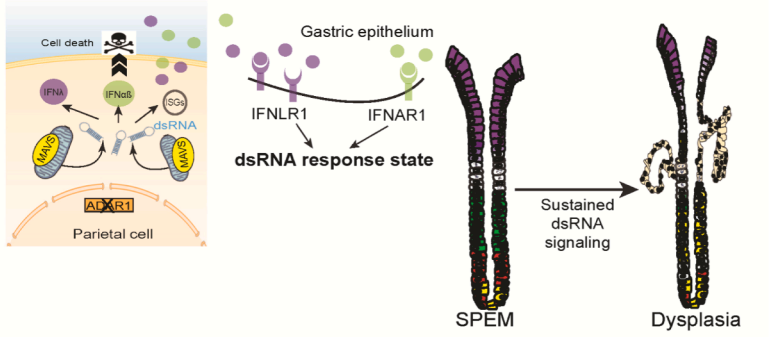

Summary We have developed and comprehensively characterized a new genetic model of gastric pre-neoplasia based on chronically dysregulated double-stranded RNA (dsRNA) signaling.

SUMMARY

The role of double-stranded RNA signaling in promoting gastric inflammation has not been directly studied. We have developed and comprehensively characterized a new genetic model of gastric pre-neoplasia based on chronically dysregulated double-stranded RNA signaling.

WHAT YOU NEED TO KNOW

Background: The response to double-stranded RNA (dsRNA) is being increasingly recognized as an innate immune signaling pathway critical to cell fate and epithelial injury.

Impact: In this study, we have developed and extensively characterized a new model of gastric pre-neoplasia based on cell-specific dysregulation of ADAR1-mediated dsRNA signaling within gastric epithelium.

Future Directions: The mechanisms by which dsRNA drives chronic inflammation likely represent an injury response that is conserved across extra-gastric epithelial tissues and that warrants future study.

BACKGROUND & AIMS: Recent evidence suggests that endogenously derived double-stranded RNA (dsRNA) impacts multiple cellular processes, although its role in epithelial injury remains understudied. We previously identified the response to dsRNA as the most upregulated pathway across 2 distinct murine models of spasmolytic polypeptide-expressing metaplasia (SPEM), a critical pre-neoplastic transition in the progression to gastric cancer. The aim of this study was to define how dysregulation of the dsRNA response within gastric epithelium impacts gastric pre-neoplasia.

METHODS: We specifically deleted ADAR1, a central regulator of dsRNA signaling, from gastric parietal cells (*Adar1*$^{\Delta PC}$).

Adar1$^{\Delta PC}$ and age-matched controls stomachs were histologically, transcriptionally, and immunologically profiled. The source of dsRNA in *Adar1*$^{\Delta PC}$ gastric epithelium was assessed by dsRNA immunoprecipitation and immuno-electron microscopy. Finally, to define the contributions of interferon (IFN) signaling, *Adar1*$^{\Delta PC}$*;Ifnar1*$^{-/-}$ *and Adar1*$^{\Delta PC}$*;Ifnlr1*$^{-/-}$ mice, defective in type I and type III IFN signaling, respectively, were characterized.

RESULTS: *Adar1*$^{\Delta PC}$ mice spontaneously developed SPEM and gastric dysplasia, in the absence of exogenous injury. Our phenotype depended on *Mavs*, a key dsRNA signaling hub, implying that our model of gastric pre-neoplasia was specific to dsRNA signaling. Further characterization of this pre-neoplastic environment by single-cell RNA sequencing and flow cytometry noted a chronic and sustained transcriptional upregulation of the dsRNA response throughout gastric epithelium that was independent of adaptive immunity and that depended on both type I and type III IFN signaling. Finally, we identified an enrichment of mitochondrial dsRNA within the gastric epithelium of *Adar1*$^{\Delta PC}$ stomachs.

CONCLUSIONS: Our new genetic model implicates ADAR1-mediated dsRNA signaling in gastric pre-neoplasia. *(Cell Mol Gastroenterol Hepatol 2026;20:101673; https://doi.org/10.1016/j.jcmgh.2025.101673)*

Keywords: ADAR1; Double-stranded RNA; Interferon.

The progression to gastric adenocarcinoma, a leading cause of global cancer deaths,[1] develops through a series of pre-neoplastic changes in the setting of chronic inflammation.[2,3] A critical transition in this neoplastic cascade is the gradual loss of acid-producing glands and the expansion of gastric epithelial progenitors, a process termed spasmolytic polypeptide-expressing metaplasia (SPEM).[4] To date, we have a limited understanding of how gastric epithelium senses and regulates cellular stress during SPEM and how these mechanisms determine whether the epithelium returns to homeostasis or progresses to cancer.

Recently, our group identified the response to double-stranded RNA (dsRNA) as the most upregulated pathway following both acute and chronic metaplastic injury in mice.[5] The accumulation of dsRNA within metaplastic gastric epithelium in both mice and humans led to activation of downstream dsRNA signaling through the production of type I interferons (IFN$\alpha\beta$) and interferon-stimulated genes (ISGs). Moreover, dsRNA was found in metaplastic stomachs of germ-free mice, suggesting that the dsRNA was not virally derived. Although the dsRNA response has often been studied in an anti-viral context,[6] multiple studies have shown that endogenously-derived dsRNA may represent a damage-associated molecular pattern (DAMP) capable of activating innate immune signaling,[7–9] implicating dsRNA as a mediator of cellular stress and as a potential driver of epithelial tumorigenesis.

Regulation of the dsRNA response occurs, in part, through the RNA editing activity of ADAR1, an RNA deaminase that catalyzes the conversion of adenosine to inosine on long strands of dsRNA.[10] ADAR1 plays critical roles in embryonic development,[8] hematopoiesis,[11] and injury-induced proliferation,[5,12,13] suggesting that the sensing and handling of dsRNA spans multiple aspects of tissue development and repair. There is increasing evidence that regulation of the dsRNA response through ADAR1 has oncogenic implications in the stomach,[7,14–16] but how dsRNA signaling in gastric epithelium promotes a pre-neoplastic environment is unknown.

To define the role of dsRNA signaling within gastric epithelium, we initially deleted *Adar1* from gastric chief cells,[5] a zymogen-producing lineage that is critical to the epithelial response to gastric injury.[17] Inducible deletion of *Adar1* from chief cells did not lead to an appreciable gastric phenotype at homeostasis.[5] As a result, we subsequently deleted *Adar1* from gastric parietal cells, a neighboring gastric epithelial lineage tasked with producing acid.[18] In contrast to chief cells, parietal cell-specific deletion of *Adar1* (*Adar1*$^{\Delta PC}$) leads to parietal cell loss as well as spontaneous SPEM and gastric dysplasia, in the absence of exogenous injury. This represents a previously unrecognized pathway in gastric pre-neoplasia resulting from cell-specific dysregulation of dsRNA signaling. Herein, we characterize the pre-neoplastic gastric environment in *Adar1*$^{\Delta PC}$ mice using transcriptional, histologic, molecular, and flow cytometric analyses. We find that dysregulated dsRNA signaling in parietal cells drives a chronic and sustained dsRNA response state throughout gastric epithelium that is independent of the adaptive immune system yet dependent on signaling through both the IFN$\alpha\beta$ receptor, IFNAR1, and the IFNλ receptor, IFNLR1. Moreover, our data demonstrate that the dsRNA that accumulates within *Adar1*-deficient gastric epithelium is lineage-specific. In particular, mitochondrial dsRNA (mt-dsRNA) is enriched in *Adar1*$^{\Delta PC}$ gastric tissue, implicating mt-dsRNA as a potential endogenous driver of innate immune signaling within the stomach. Our new in vivo model underscores essential roles for dsRNA signaling in gastric pre-neoplasia.

Abbreviations used in this paper: **ANOVA, analysis of variance; BSA, bovine serum albumin; CPM, count-per-million; DAMP, damage-associated molecular pattern; DAPI, 4',6-diamidino-2-phenylindole; DEG, differentially expressed gene; DMEM, Dulbecco's Modified Eagle's Medium; dsRIP, dsRNA immunoprecipitation; dsRNA, double-stranded RNA; DTT, dithiothreitol; E, embryonic day; ECL, enterochromaffin-like cell; FACS, fluorescence-activated cell sorting; FBS, fetal bovine serum; HD-Tam, high-dose tamoxifen; IFN, interferon; IFN$\alpha\beta$, type I interferons; IFNλ, type III interferons; ISG, interferon-stimulated gene; KO, Adar1-deficient; MAVS, mitochondrial anti-viral signaling protein; mt-dsRNA, mitochondrial dsRNA; P, post-natal day; PBS, phosphate buffered saline; PCA, principal component analysis; qRT-PCR, quantitative reverse transcription-polymerase chain reaction; RNA-seq, RNA sequencing; scRNA-seq, single cell RNA-sequencing; SD, standard deviation; SEM, standard error of the mean; SPEM, spasmolytic polypeptide-expressing metaplasia; SSC, saline sodium citrate; TCGA, The Cancer Genome Atlas; TUNEL, terminal deoxynucleotidyl transferase dUTP nick-end labeling; UMAP, Uniform Manifold Approximation and Projection; WT, Adar1-sufficient.**


Most current article

© 2025 The Authors. Published by Elsevier Inc. on behalf of the AGA Institute. This is an open access article under the CC BY-NC-ND license (http://creativecommons.org/licenses/by-nc-nd/4.0/).

2352-345X
https://doi.org/10.1016/j.jcmgh.2025.101673

Results

Loss of Adar1 From Parietal Cells Leads to Oxyntic Atrophy

To assess how dysregulation of dsRNA signaling affects gastric epithelium, we specifically deleted *Adar1*, a key regulator of the dsRNA response,[10] from gastric parietal cells by crossing *Adar1*-floxed mice (*Adar1*$^{fl/fl}$)[19] to mice with a parietal cell-specific *Atp4b*^{Cre} allele bearing an *Ai9* reporter (*ROSA26*^{LSLtdTomato}). We refer to these mice as *Adar1*$^{\Delta PC}$ (Figure 1*A*). As expected, Cre recombination was specific to parietal cells of the gastric corpus (Figure 1*B*). *Atp4b*^{Cre} expression could be detected as early as embryonic day 17.5 (E17.5) and was observed in nascent gastric glands at postnatal day 1 (P1) (Figure 1*C*). When comparing the stomachs of control and *Adar1*$^{\Delta PC}$ mice at these early developmental stages, no notable histologic differences were seen in terms of parietal cell numbers, gastric epithelial proliferation, or gastric epithelial cell death (Figure 1*D*). However, as the number of parietal cells in control mice gradually increased over the first year of life, the stomachs of *Adar1*$^{\Delta PC}$ mice were persistently depleted of parietal cells over the same time period (Figure 1*E*). Specifically, the parietal cell census between control and *Adar1*$^{\Delta PC}$ stomachs diverged by 2 weeks of age, with a clear reduction in parietal cell numbers in *Adar1*$^{\Delta PC}$ stomachs compared with control stomachs (Figure 1*E–F*).

To establish a role for *Adar1* and dsRNA signaling in parietal cell development, we performed bulk RNA sequencing (RNA-seq) on stomachs isolated from control and *Adar1*$^{\Delta PC}$ mice at E17.5, P1, and P15 time points. Control and *Adar1*$^{\Delta PC}$ stomachs showed significant transcriptional similarities early in development, with few genes being differentially expressed between the 2 genotypes at these developmental time points (Figure 1*G*), consistent with what was observed histologically (Figure 1*D–E*). However, by 2 weeks of age, the number of differentially expressed genes (DEGs) between control and *Adar1*$^{\Delta PC}$ stomachs was considerably higher (Figure 1*G*). Pathway analysis of DEGs showed that, although both control and *Adar1*$^{\Delta PC}$ stomachs expressed genes associated with developmental pathways during early development (ie, E17.5), *Adar1*$^{\Delta PC}$ stomachs were transcriptionally skewed toward activation of dsRNA signaling and the interferon (IFN) response later in development (ie, P15) (Figure 1*H*). By 2 weeks of age, the gastric corpora of control mice were primarily characterized by pathways associated with parietal cell function (eg, aerobic respiration, electron transport) (Figure 1*H*), whereas the gastric corpora of *Adar1*$^{\Delta PC}$ mice showed activation of the dsRNA response (Figure 1*H*), which was confirmed by quantitative reverse transcription-polymerase chain reaction (qRT-PCR) (Figure 1*I*). Together, these data suggest that *Adar1* alters the developmental trajectory of parietal cells within the first 2 weeks of postnatal stomach development.

Parietal Cell Loss in Adar1$^{\Delta PC}$ Stomachs Is Independent of Adaptive Immunity

Consistent with the sustained depletion of parietal cells in *Adar1*$^{\Delta PC}$ stomachs (Figure 1*E*), *Adar1*$^{\Delta PC}$ gastric glands demonstrated markers of apoptosis, including increased terminal deoxynucleotidyl transferase dUTP nick-end labeling (TUNEL) staining (Figure 2*A–B*) and cleaved caspase 3 expression (Figure 2*C*), as well as of necroptosis, as seen by increased phospho-MLKL expression[21] (Figure 2*D*), at 8 weeks of age. As immune cells and their cytokines are known to be potent inducers of epithelial cell death,[22,23] we initially hypothesized that infiltrating immune cells were contributing to parietal cell loss. Parietal cell numbers between control and *Adar1*$^{\Delta PC}$ mice diverged by 2 weeks of age (Figure 1*E–F*), which would correlate with development of the murine immune system.[24] To test whether parietal cell loss and the observed gastric pathology in *Adar1*$^{\Delta PC}$ stomachs depended on immune-mediated effects, we crossed *Adar1*$^{\Delta PC}$ mice to *Rag1*-deficient mice, which are devoid of functional B and T cells.[25] As expected, *Rag1*$^{-/-}$ and *Adar1*$^{\Delta PC}$;*Rag1*$^{-/-}$ mice showed no detectable B and T cells in gastric mucosa (Figure 2*E–F*) or in spleen (data not shown). *Adar1*$^{\Delta PC}$;*Rag1*$^{-/-}$ mice demonstrated significant increases in F480^{+} macrophages and Ly6c^{+} monocytes in gastric corpus mucosa, compared with *Adar1*$^{\Delta PC}$ stomachs (Figure 2*G*). Importantly, *Adar1*$^{\Delta PC}$;*Rag1*$^{-/-}$ mice showed a depletion of parietal cells (Figure 2*H–I*) and upregulation of the dsRNA response at the transcriptional (Figure 2*J*) and protein (Figure 2*K*) levels, demonstrating that oxyntic atrophy and activation of the dsRNA response in *Adar1*$^{\Delta PC}$ stomachs are independent of B/T cell signaling.

Adar1$^{\Delta PC}$ Mice Spontaneously Develop SPEM

Because parietal cell loss is a critical early step in establishing SPEM,[26,27] a gastric pre-neoplastic stage, we wanted to histologically assess for the development of SPEM in *Adar1*$^{\Delta PC}$ stomachs. Indeed, compared with age-matched control stomachs, *Adar1*$^{\Delta PC}$ stomachs demonstrated hallmark features of SPEM, including the expression of metaplastic markers (ie, coexpression of chief cell and mucous neck cell markers, CD44v10 expression[28]) (Figure 3*A–B*) and increased epithelial proliferation (ie, Ki-67) (Figure 3*C–D*).[29] Together, our findings demonstrate that specific loss of *Adar1* from a single gastric epithelial lineage is sufficient to induce SPEM, in the absence of exogenous injury.

Oxyntic Atrophy and SPEM in Adar1$^{\Delta PC}$ Stomachs Depend on dsRNA Signaling Through MAVS

Following the recognition of cytosolic dsRNA, the sensors DDX58 (RIG-I) and IFIH1 (MDA5) converge on Mitochondrial Anti-Viral Signaling protein (MAVS), a mitochondrially or peroxisomally tethered signaling hub through which the dsRNA response is transduced (Figure 4*A*).[30–33] To demonstrate that oxyntic atrophy and SPEM in *Adar1*$^{\Delta PC}$ stomachs depended on dsRNA signaling, we transcriptionally and histologically compared *Adar1*$^{\Delta PC}$ stomachs with age-matched *Adar1*$^{\Delta PC}$ stomachs deficient in MAVS signaling (*Adar1*$^{\Delta PC}$;*Mavs*$^{-/-}$). In the absence of *Mavs*, the transcriptional dsRNA response was blocked (Figure 4*B*). Accordingly, *Adar1*$^{\Delta PC}$;*Mavs*$^{-/-}$ mice did not

develop any of the histologic changes consistent with oxyntic atrophy or with SPEM (Figure 4*C*), as was seen in age-matched *Adar1*$^{\Delta PC}$ stomachs. Our data therefore illustrate a rescue of oxyntic atrophy/SPEM and demonstrate that the gastric pathology observed in *Adar1*$^{\Delta PC}$ mice depends on dsRNA signaling through MAVS.

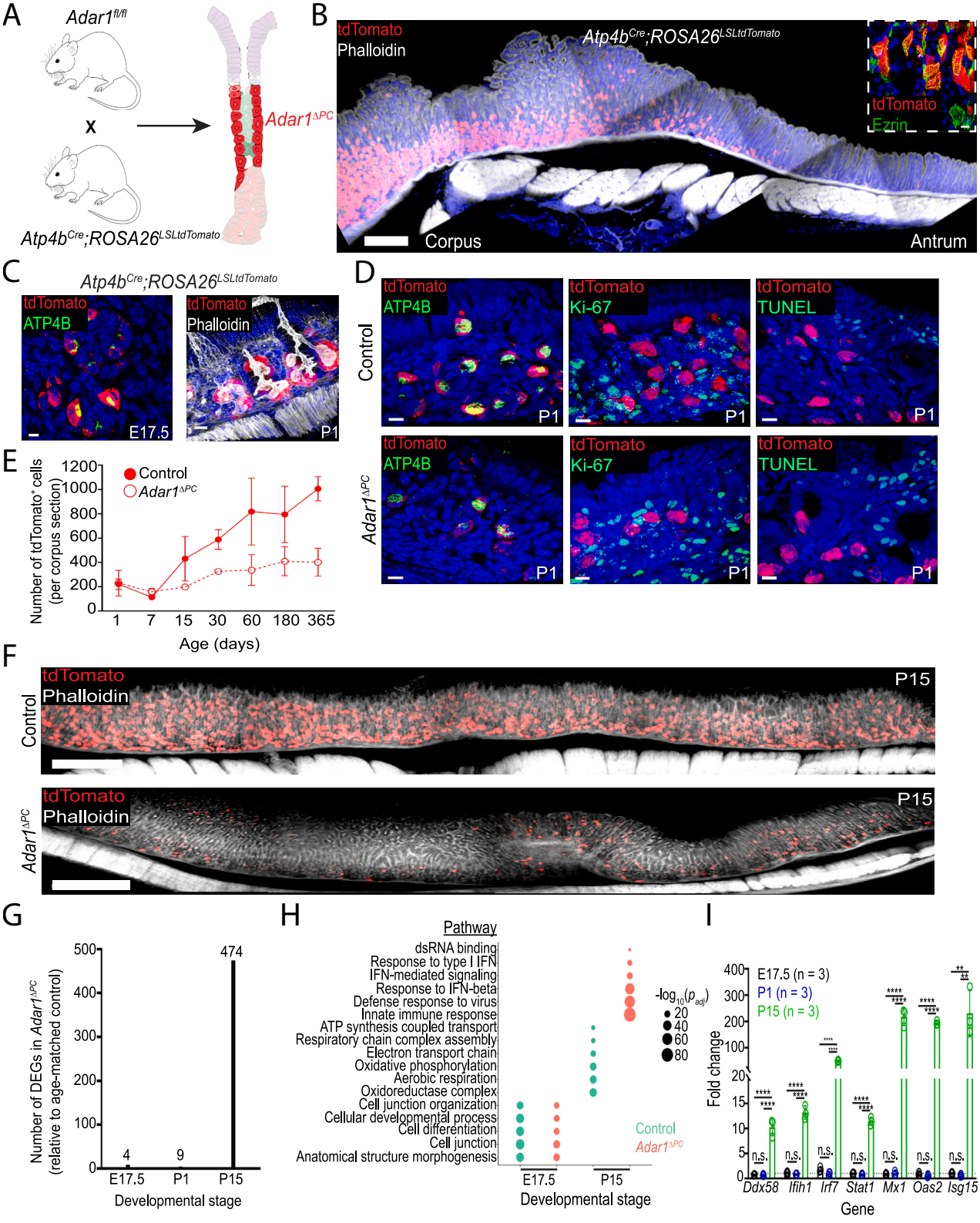

Mitochondrial dsRNA Specifically Accumulates Within Mavs-deficient Adar1$^{\Delta PC}$ Gastric Epithelium

Based on our findings, we wanted to determine the cellular source(s) of dsRNA that mediates gastric pathology through MAVS signaling. In addition to *Mavs*-deficient *Adar1*$^{\Delta PC}$ mice (*Adar1*$^{\Delta PC}$;*Mavs*$^{-/-}$) being protected from gastric pathology (Figure 4*C*), we noted an accumulation of dsRNA in the gastric epithelium of these mice, compared with *Adar1*$^{\Delta PC}$ stomachs (Figure 4*D*). This suggested that the dsRNA that accumulates in *Adar1*$^{\Delta PC}$;*Mavs*$^{-/-}$ stomachs triggers downstream dsRNA signaling through MAVS. To identify the type(s) of dsRNA that accumulates in *Adar1*$^{\Delta PC}$;*Mavs*$^{-/-}$ stomachs, we immunoprecipitated dsRNA from gastric corpus lysates of *Adar1*$^{\Delta PC}$;*Mavs*$^{-/-}$ (experimental) and *Adar1*$^{fl/fl}$;*Mavs*$^{-/-}$ (control) mice. In this experiment, both control and experimental mice cannot signal through MAVS but differ only in that the experimental group lacks *Adar1* in parietal cells. Input and eluted RNA were analyzed by RNA-seq (Figure 4*E*). Pull-down with control IgG did not yield sufficient high-quality RNA for sequencing (data not shown). After normalizing for input, *Adar1*$^{\Delta PC}$;*Mavs*$^{-/-}$ stomachs were enriched for mt-dsRNA, compared with control stomachs. Of the 10 most upregulated protein-coding transcripts, 5 were mitochondrial (Figure 4*F*). To confirm our findings, immuno-electron microscopic labeling demonstrated the accumulation of dsRNA within the mitochondria of parietal cells in *Adar1*$^{\Delta PC}$;*Mavs*$^{-/-}$ stomachs but not in control stomachs (Figure 4*G*).

To determine whether the accumulation of mt-dsRNA was cell-specific and not simply the result of *Adar1* deficiency, we compared dsRNA immunoprecipitated from *Adar1*$^{\Delta PC}$;*Mavs*$^{-/-}$ stomachs, which lack *Adar1* in parietal cells, with dsRNA immunoprecipitated from *Adar1*$^{fl/fl}$;*Mist1*$^{Cre\text{-}ERT/+}$ stomachs, which lack *Adar1* in chief cells (*Adar1*$^{\Delta CC}$), a different epithelial lineage of the gastric corpus.[17] We had previously shown that the inducible deletion of *Adar1* from chief cells led to the accumulation of gastric epithelial dsRNA.[5] However, sequencing of dsRNA immunoprecipitated from *Adar1*$^{\Delta CC}$ stomachs (Figure 4*I*) did not show the same enrichment for mt-dsRNA that was observed in *Adar1*$^{\Delta PC}$;*Mavs*$^{-/-}$ stomachs (Figure 4*H*), suggesting that the accumulation of mt-dsRNA is specific to *Adar1*-deficient parietal cells. Despite an accumulation of mt-dsRNA in *Adar1*-deficient parietal cells (Figure 4*F–G*), differential expression analyses between *Adar1*-sufficient and *Adar1*-deficient parietal cells, isolated by fluorescence-activated cell sorting (FACS) (Figure 4J), showed a relative decrease in mitochondrial transcripts and a relative upregulation of metaplastic transcripts in *Adar1*-deficient parietal cells compared with *Adar1*-sufficient parietal cells (Figure 4*K*).

Characterization of the ADAR1 Editome in Gastric Epithelium

The observed gastric phenotype in *Adar1*$^{\Delta PC}$ mice was independent of B/T cell signaling (Figure 2), so we hypothesized that endogenous, cell-intrinsic mechanisms could be mediating the effects of *Adar1* loss. ADAR1 modulates the response to endogenous dsRNA through RNA editing,[10,34] but cell-specific differences in ADAR1 editing are largely unknown. To determine whether ADAR1 editing (or loss of editing) contributed to our phenotype, we sought to correlate ADAR1-mediated A-to-I editing with gene expression in parietal cells. We first performed RNA sequencing on both *Adar1*-sufficient (WT) or -deficient (KO) parietal cells, which were isolated by tdTomato expression, using FACS (Figure 4*J*). Of note, both WT and KO parietal cells were *Mavs*-deficient (*Mavs*$^{-/-}$), which allowed for the isolation of viable KO parietal cells (Figure 4*C*) and which maximized the accumulation of dsRNA (Figure 4*D–E*). Next, we defined the ADAR1 editome in parietal cells. We identified sites that were specifically edited by ADAR1 using a modified analysis pipeline (see Methods). We selected sites where the A-to-I editing

Figure 1. (***See previous page***). **The effects of *Adar1* loss from parietal cells.** (*A*) *Adar1*$^{\Delta PC}$ mice were generated by crossing *Adar1*-floxed mice (*Adar1*$^{fl/fl}$) mice to *Atp4b*^{Cre} mice bearing a *ROSA26*^{LSLtdTomato} reporter. (*B*) Cre recombinase expression (tdTomato, *red*) is specific to parietal cells of the gastric corpus. Representative confocal image of a *Atp4b*^{Cre};*ROSA26*^{LSLtdTomato} mouse stomach (8 weeks of age) spanning corpus to antrum is shown. Scale bar, 100 μm. Inset shows coexpression of the tdTomato reporter (*red*) with adult parietal cells, marked by ezrin expression (*green*). Scale bar, 10 μm. (*C*) *Atp4b*^{Cre} expression (*red*) is detected as early as E17.5 (*left*) and can be seen in nascent gastric glands at P1 (*right*). Scale bars, 5 μm. (*D*) Representative confocal images of P1 stomachs from control (*top*) and *Adar1*$^{\Delta PC}$ (*bottom*) mice demonstrate similar ATP4B-expressing parietal cell census (*left*), gastric epithelial proliferation (*green*; *middle*), and gastric epithelial apoptosis (TUNEL staining, *green*; *right*). Scale bars, 10 μm. (*E*) tdTomato^{+} parietal cells were quantified from the glandular stomachs or gastric corpora of control (*solid*) and *Adar1*$^{\Delta PC}$ (*open*) stomachs over time. Mean ± SEM tdTomato^{+} parietal cells per corpus section (3–4 corpus sections per mouse, n = 5 mice/genotype/time point) are shown at the indicated ages. Quantification was performed by an investigator blinded to the genotypes. (*F*) Representative gastric corpus sections showing a depletion of parietal cells (*red*) in *Adar1*$^{\Delta PC}$ stomachs (*bottom*) compared with control stomachs (*top*) at P15. Scale bars, 200 μm. (*G*) The number of differentially expressed genes (DEGs) in *Adar1*$^{\Delta PC}$ stomachs, relative to control stomachs, at each development stage is shown. Gene expression (n = 3 mice/genotype) was determined by RNA-seq of glandular stomachs (E17.5) or of gastric corpora (P15). The cutoffs for differential expression were defined as a linear fold change of ±1.5 and $P < .05$. (*H*) Dot plots of enriched pathways in control and *Adar1*$^{\Delta PC}$ stomachs, based on developmental stage. Pathway analyses (using gProfiler[20]) were performed based on genes significantly upregulated at E17.5 (relative to P15) or at P15 (relative to E17.5) for each genotype. (*I*) The dsRNA response is transcriptionally upregulated at P15 in *Adar1*$^{\Delta PC}$ stomachs. Bars represent mean ± SD fold change expression (by qRT-PCR) in *Adar1*$^{\Delta PC}$ stomachs, relative to age-matched controls. Each data point is an individual mouse stomach. The number of mice per genotype is shown in parentheses. Comparisons were made by one-way ANOVA with post-hoc Tukey tests. $^{**}P < .01$; $^{****}P < .0001$; n.s., not significant ($P > .05$).

frequency was >5% in *Adar1*-sufficient parietal cells (WT) and was reduced to <1% at that same site in *Adar1*-deficient parietal cells (KO) (Figure 5*A*). Indeed, parietal cells with intact ADAR1 (WT) showed variable editing frequency, whereas parietal cells lacking ADAR1 (KO) showed little to no editing at the corresponding sites (Figure 5*B–D*), confirming

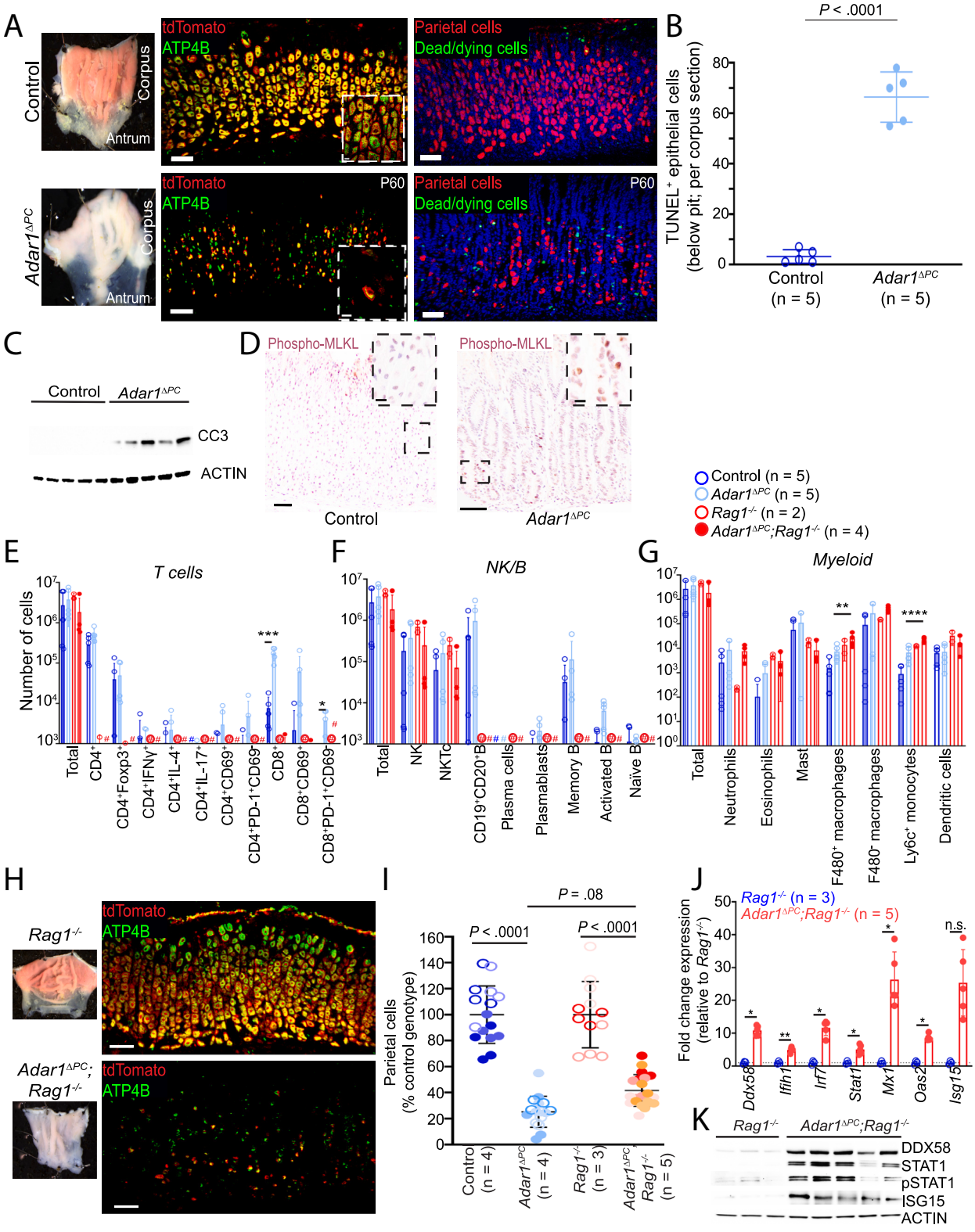

that editing at these sites was ADAR1-dependent. Consistent with previous studies,[9,34] nearly one-half of ADAR1-edited sites in parietal cells occurred at 3′-UTR regions (Figure 5*E*). Loss of ADAR1 editing in parietal cells correlated with increased expression of certain genes (eg, *Lgr4*, *Arhgap11*, *Galntl6*), whereas the expression of other genes was reduced in the absence of ADAR1 editing (eg, *Lpl, Nmnat1*, *Nfs1*) (Figure 5*F*). Although mitochondrial transcripts were significantly downregulated in *Adar1*-deficient parietal cells (Figure 4*K*), they were not edited by ADAR1 to an appreciable extent (Figure 5*F*, *boxed area*).

Adar1$^{\Delta PC}$ Stomachs Are Characterized by a Glandular dsRNA Response State

To define how the dsRNA response contributed to gastric pre-neoplasia, we transcriptionally characterized control and *Adar1*$^{\Delta PC}$ stomachs by single cell RNA-sequencing (scRNA-seq) of gastric corpus tissue at 8 weeks of age (Figure 6*A*). We confirmed the presence of all expected epithelial and nonepithelial cell populations of the gastric corpus, based on known and validated transcriptional markers (Figure 6*B–C*).[35,36] Based on these markers, we compared the census of cell populations between control and *Adar1*$^{\Delta PC}$ stomachs. Consistent with our histologic findings (Figure 3), *Adar1*$^{\Delta PC}$ stomachs had fewer parietal cells and chief cells, an expansion of proliferative cells, and the emergence of metaplastic populations (Figure 6*A, D–E*).

Our analyses identified 2 distinct metaplastic populations, one which we defined as SPEM and which was characterized by established and validated SPEM transcripts (eg, *Aqp5*, *Gkn3*, *Wfdc2*, *Dmbt1*),[35] the other which we named "metaplasia-like" and which was characterized by varied expression of multiple epithelial lineages, including transcripts from SPEM cells (eg, *Aqp5*), foveolar cells (eg, *Muc5ac*), parietal cells (eg, *Atp4b*), chief cells (eg, *Pdia2*), and even enterochromaffin-like cells (ECLs; eg, *Chga*) (Figure 6*C*). In addition, we identified a novel population, which we named "pancreatic acinar-like," that was characterized by pancreatic acinar transcripts (eg, *Ctrb1*, *Cpa1*) (Figure 6*A–C*). This population, however, did not express pancreatic acinar proteins typically seen in pancreatic metaplasia (data not shown). Moreover, this population was only seen in *Adar1*$^{\Delta PC}$ stomachs at 8 weeks of age but could not be identified at later time points (Figure 8*B, E*). The "pancreatic acinar-like" and "metaplasia-like" populations could therefore represent transient cell populations marked by transcriptional sampling, highlighting the cellular plasticity that has been observed in gastric epithelium during injury.[37]

To establish how the cell-specific loss of *Adar1* from parietal cells contributed to SPEM, we compared the transcriptional profiles between *Adar1*-sufficient (control) and *Adar1*-deficient (*Adar1*$^{\Delta PC}$) parietal cells from scRNA-seq data. Interestingly, *Adar1*-deficient parietal cells downregulated expression of genes typically associated with parietal cell function (ie, electron transport, oxidative phosphorylation) and acid secretion,[38] and skewed toward expression of dsRNA response genes (Figure 7*A*). More importantly, this transcriptional signature extended beyond parietal cells and was observed throughout multiple gastric epithelial lineages (Figure 7*B–E*). Finally, protein expression of multiple components of the dsRNA response was upregulated in gastric corpus tissue of *Adar1*$^{\Delta PC}$ mice (Figure 7*F*). These findings collectively demonstrate that loss of *Adar1* from parietal cells leads to a glandular dsRNA response state.

Sustained dsRNA Signaling in *Adar1*$^{\Delta PC}$ Mice Leads to Gastric Dysplasia

To examine the progression of SPEM in *Adar1*$^{\Delta PC}$ stomachs, we aged *Adar1*$^{\Delta PC}$ mice to 12 months. Compared

Figure 2. (***See previous page***). **Parietal cell loss in *Adar1*$^{\Delta PC}$ mice is independent of adaptive immunity.** (*A*) Oxyntic atrophy is observed by gross morphology (*left*) in *Adar1*$^{\Delta PC}$ stomachs (*bottom*) at 8 weeks of age (P60), compared with age-matched control stomachs (*top*). Histologically, parietal cell loss (*middle*) and increased apoptosis (TUNEL stain, *green*; *right*) can also be seen. Scale bars, 50 μm and 10 μm (*insets*). (*B*) Quantification of TUNEL-positive epithelial cells in control and *Adar1*$^{\Delta PC}$ stomachs at 8 weeks of age. Mean ± SD TUNEL-positive epithelial cells below the pit region per corpus section of an individual mouse (n = 5 mice/genotype) are shown. Comparisons were made using the Student's *t*-test. (*C*) Western blot demonstrating increased cleaved CASPASE 3 (CC3) expression in *Adar1*$^{\Delta PC}$ stomachs at 8 weeks of age, compared with control stomachs. Each lane represents gastric corpus tissue from an individual mouse at 8 weeks of age. (*D*) *Adar1*$^{\Delta PC}$ stomachs (*right*) show increased expression of the necroptotic marker, phospho-MLKL, at 8 weeks of age, compared with age-matched control stomachs (*left*). Boxed areas are magnified. Scale bars, 50 μm and 10 μm (*boxed*). (*E–G*) Flow cytometry of T cells (*E*), NK/B cells (*F*), and myeloid cells (*G*) isolated from gastric corpus mucosa. Bars represent mean ± SD. Each data point is an individual mouse at 8 weeks of age. Numbers of mice per genotype are in parentheses. Immune cell populations were compared between genotypes by 1-way ANOVA with post-hoc Tukey tests. #, not detected. $^{**}P < .01$; $^{***}P < .001$; $^{****}P < .0001$. NK, natural killer. (*H*) Parietal cell loss is independent of B/T cell signaling. Representative gross morphologic (*left*) and immunofluorescent (*right*) images of gastric corpus sections are shown. Scale bars, 50 μm. (*I*) The number of tdTomato^{+} cells was counted for 4 randomly selected high-powered fields (20×) for each mouse. The means ± SEM for each genotype are shown. Each color corresponds to a different mouse. Numbers of mice per genotype are provided in parentheses. Data are expressed as percent of control genotype. Quantification was performed by a researcher blinded to the genotypes. Comparisons were made by ANOVA with post-hoc Tukey tests, and *P* values are provided. (*J*) The dsRNA response is transcriptionally upregulated in *Adar1*$^{\Delta PC}$;*Rag1*$^{-/-}$ mice (*red*), compared with age-matched *Rag1*$^{-/-}$ controls (*blue*). Bars represent mean ± SD fold change expression (by qRT-PCR), relative to age-matched *Rag1*$^{-/-}$ controls. Each data point is an individual gastric corpus section. Numbers of mice per genotype are shown in parentheses. Dotted line represents average expression in *Rag1*$^{-/-}$ stomachs. Comparisons were made by the Student's *t*-test. $^{*}P < .05$; $^{**}P < .01$; n.s., not significant ($P > .05$). (*K*) Western blot demonstrating activation of the dsRNA response in *Adar1*$^{\Delta PC}$;*Rag1*$^{-/-}$ stomachs. Each lane represents gastric corpus tissue from an individual mouse at 8 weeks of age. pSTAT1, phospho-STAT1.

with age-matched control stomachs, *Adar1*$^{\Delta PC}$ stomachs showed cyst-like, distorted glandular architecture (Figure 8*A*). The sustained depletion of parietal cells and expansion of metaplastic and proliferative cells was confirmed by scRNA-seq (Figure 8*B*). Similar to *Adar1*$^{\Delta PC}$ stomachs at 8 weeks of age (Figure 7*D–F*), the stomachs of

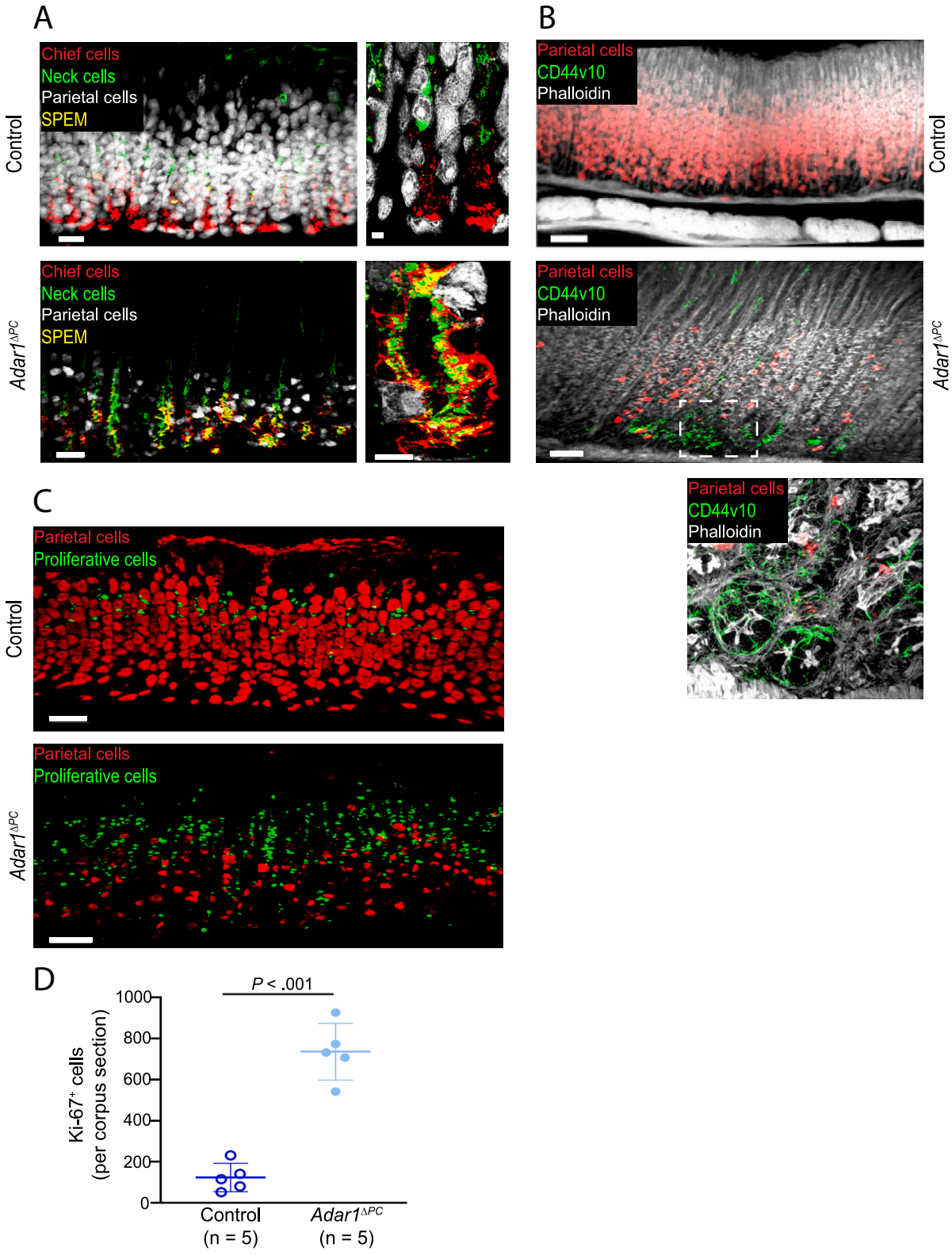

Adar1$^{\Delta PC}$ mice at 12 months of age demonstrated an upregulation of the glandular dsRNA response, both at the transcriptional (Figure 8*C*) and protein (Figure 8*D*) levels. The transcriptional upregulation of dsRNA response genes (eg, *Ifit1*, *Isg15*, *Irf7*) within gastric epithelium, coupled with the downregulation of parietal (eg, *Hamp2*, *Fabp3*) and chief cell genes (eg, *Chia1*, *Pla2g1b*), was sustained from 8 weeks to 12 months of age (Figure 8*E*).

Importantly, *Adar1*$^{\Delta PC}$ stomachs developed gastric dysplasia by 12 months of age, marked by expression of the validated dysplastic marker, TROP2[40] (Figure 8*F–G*). The observed dysplasia in *Adar1*$^{\Delta PC}$ stomachs was not simply the result of oxyntic atrophy or gastric inflammation, as established models of acute/chronic gastric injury (ie, high-dose tamoxifen,[41] *Helicobacter pylori* infection[42]) and of parietal cell depletion (ie, Diphtheria toxin-induced parietal cell loss[43]) did not lead to enhanced TROP2 expression (Figure 8*H*). At 12 months of age, TROP2-positive gastric epithelium tended to be distinct from CD44v10-positive gastric epithelium (Figure 8*I*). The progression from SPEM to dysplasia in *Adar1*$^{\Delta PC}$ stomachs therefore correlates with a chronic and sustained activation of the dsRNA response.

Next, we hypothesized that differentially expressed pathways in *Adar1*$^{\Delta PC}$ stomachs between 8 weeks and 12 months would allow us to uncover pathways involved in the progression from SPEM (ie, 8 weeks) to gastric dysplasia (ie, 12 months), in the setting of a sustained dsRNA response state. Similarly, differentially expressed pathways shared among multiple epithelial lineages would suggest epithelium-autonomous dysplastic pathways. Although there were no pathways that were upregulated at 12 months (relative to 8 weeks) and shared among the select epithelial lineages, the progression from SPEM to gastric dysplasia was characterized by shared downregulation of the SWI/SNF complex assembly pathway (Figure 9*A*), which has been shown to function as a tumor suppressive pathway in multiple malignancies, including human gastric cancer.[44] Downregulation of multiple components of this tumor suppressive pathway (eg, *Arid1a*, *Arid1b*, *Pbrm1*) was confirmed across the studied epithelial populations (Figure 9*B*) and by immunohistochemistry (eg, ARID1A) (Figure 9*C–D*). Consistent with the tumor suppressive role of the SWI/SNF complex assembly pathway, decreased expression of some members of this pathway significantly correlated with decreased overall survival in human gastric cancer (Figure 9*E–F*).

To establish whether this new murine model of gastric dysplasia shared transcriptional features with human gastric adenocarcinoma, we identified a subset of genes with increased epithelial expression in dysplastic *Adar1*$^{\Delta PC}$ stomachs that were similarly upregulated across different human gastric cancer molecular subtypes (Figure 9*G*), based on cross-referencing with The Cancer Genome Atlas (TCGA).[47] A dysplasia signature score based on these human gastric cancer genes showed increased expression among a subset of foveolar cells in *Adar1*$^{\Delta PC}$ stomachs at 12 months of age (Figure 9*H–I*; *arrowhead*). Our murine model of gastric dysplasia therefore shares transcriptional features with human gastric adenocarcinoma.

The dsRNA Response State in *Adar1*$^{\Delta PC}$ Stomachs Depends on Type I and Type III IFN Signaling

Activation of the dsRNA response leads to the production of type I (IFN$\alpha\beta$)[22] and type III (IFNλ)[48] IFNs, which signal through the IFNAR1/2[49] and IFNLR1/IL-10RB[50] receptors, respectively. Given that the dsRNA response stimulates type I and type III IFNs and that *Adar1*$^{\Delta PC}$ stomachs show chronic stimulation of the dsRNA response, we reasoned that gastric pathology observed in *Adar1*$^{\Delta PC}$ stomachs was mediated, in part, by type I and/or type III IFN signaling. To test how each arm of IFN signaling contributed to gastric pathology in *Adar1*$^{\Delta PC}$ mice, we first crossed *Adar1*$^{\Delta PC}$ mice to *Ifnar1*$^{-/-}$ mice, which are deficient in type I (IFN$\alpha\beta$) signaling through the IFNAR1/2 receptor. We had previously confirmed that the gastric epithelium of *Ifnar1*$^{-/-}$ mice is indeed insensitive to IFNβ.[5] As with *Adar1*$^{\Delta PC}$ mice, *Adar1*$^{\Delta PC}$;*Ifnar1*$^{-/-}$ mice were characterized by oxyntic atrophy and SPEM (Figure 10*A–B*), as well as by upregulation of the dsRNA response at the transcriptional (Figure 10*F*) and protein (Figure 10*G*) levels. Similarly, *Adar1*$^{\Delta PC}$;*Ifnlr1*$^{-/-}$ mice, generated by crossing *Adar1*$^{\Delta PC}$ mice to *Ifnlr1*$^{-/-}$ mice, which are deficient in type III (IFNλ) signaling through the IFNLR1 receptor, also demonstrated oxyntic atrophy and SPEM (Figure 10*C–D*), in addition to activation of the dsRNA response (Figure 10*F–G*). Interestingly, however, *Adar1*$^{\Delta PC}$ mice deficient in both type I and type III IFN signaling (*Adar1*$^{\Delta PC}$;*Ifnar1*$^{-/-}$;*Ifnlr*$^{-/-}$) were completely protected from parietal cell loss and SPEM (Figure 10*E*). More importantly, the dsRNA response in these mice was completely blocked (Figure 10*F–G*). Taken together, the chronically sustained dsRNA response state in the stomachs of *Adar1*$^{\Delta PC}$ mice leads to gastric pre-neoplastic changes that depend on both type I and type III IFN signaling (Figure 10*H*).

Discussion

The accumulation of endogenously derived dsRNA has been increasingly recognized as an indicator of cellular

Figure 3. (***See previous page***). ***Adar1***$^{\Delta PC}$ **mice develop SPEM.** (*A*) Compared with control mice (*top*), *Adar1*$^{\Delta PC}$ stomachs (*bottom*) show histologic hallmarks of SPEM, including a depletion of parietal cells (*white*) and coexpression (*yellow*) of chief cell (GIF, *red*) and mucous neck cell (GSII, *green*) markers at gland bases. Images represent mice at 8 weeks of age. Scale bars, 20 μm and 5 μm (*right*). GIF, gastric intrinsic factor; GSII, *Griffonia simplicifolia* II. (*B*) *Adar1*$^{\Delta PC}$ stomachs (*bottom*) show increased expression of the metaplastic marker, CD44v10 (*green*), extending down to gland bases (*boxed area*). A magnified gland base is shown. Scale bars, 50 μm. (*C*) Epithelial proliferation (Ki-67; *green*) is enhanced along the gland axis in *Adar1*$^{\Delta PC}$ stomachs (*bottom*). Scale bars, 50 μm. (*D*) Quantification of gastric epithelial proliferation. Data points represent mean ± SD Ki-67-positive cells per corpus section from an individual mouse (n = 5 mice/genotype). Comparisons were performed using the Student's *t*-test. Quantification was performed by a researcher blinded to the genotypes.

stress.[9] It has also become apparent that the ability to appropriately sense and respond to endogenous dsRNA is critical to development,[8] homeostasis,[11] and injury,[5,12,13] but how dysregulation of dsRNA signaling contributes to epithelial injury and pre-neoplasia has not been directly investigated. Some studies have indirectly implicated

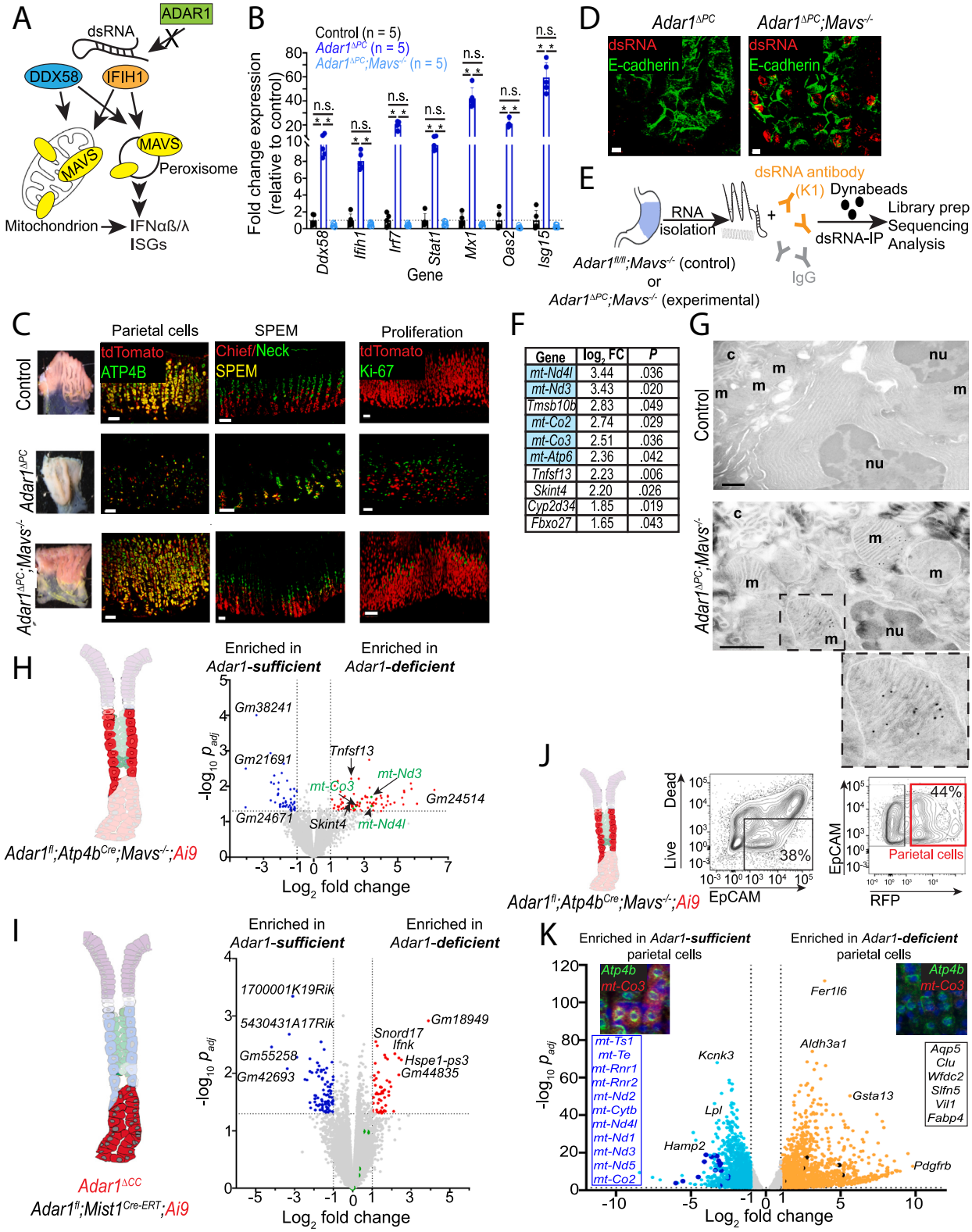

dsRNA/IFN signaling in human gastric tumorigenesis,[7,14] but whether dsRNA is a byproduct or driver of a pro-tumorigenic environment is not known. Interestingly, *Adar1*$^{\Delta PC}$ mice, despite showing characteristic changes of SPEM and gastric dysplasia, did not show any histologic or transcriptional evidence of gastric intestinal metaplasia, a known pre-neoplastic stage,[3] at any of the time points studied (data not shown). The reasons for this are unclear and are currently being studied. Regardless, in this study, we demonstrate that dysregulation of the dsRNA response through targeted in vivo deletion of *Adar1* from a single gastric epithelial lineage is sufficient to produce a sustained dsRNA response that leads to pre-neoplastic changes (ie, SPEM, gastric dysplasia), in the absence of exogenous injury. This new in vivo model of gastric pre-neoplasia depends on signaling through MAVS. Interestingly, the sustained dsRNA response is independent of B/T cell signaling, although whether the glandular response relies on myeloid cells (eg, F480^{+} macrophages, Ly6c^{+} monocytes) or on epithelium-autonomous paracrine signals is not known. More importantly, we demonstrate that the pre-neoplastic environment that develops in *Adar1*$^{\Delta PC}$ stomachs is characterized by a dsRNA response state that is expressed throughout the gastric gland and is entirely dependent on both type I and type III IFN signaling. Future studies are needed to determine the relative contributions of each arm of the IFN response; in particular, the role of type III IFN signaling to the gastric pre-neoplastic microenvironment.

ADAR1-mediated editing of endogenously derived dsRNA alters its recognition by cytosolic dsRNA sensors and modulates downstream signaling.[32] We report, for the first time, the ADAR1-dependent RNA editome of a distinct gastric epithelial lineage (ie, parietal cells) in vivo. More importantly, the ability to characterize the ADAR1 editome within parietal cells allows us to infer how cell-specific differences in dsRNA accumulation and ADAR1 editing correlate with cell fate and glandular injury. For one, the source of dsRNA seems to be cell-dependent. *Adar1*$^{\Delta PC}$*;Mavs*$^{-/-}$ stomachs, which fail to activate the dsRNA response and are protected from gastric pathology, accumulate mt-dsRNA, so we reasoned that this unedited mt-dsRNA drives the dsRNA response. Interestingly, mt-dsRNA accumulated when *Adar1* was specifically deleted from parietal cells but not from chief cells. One potential explanation is that parietal cells inherently have more mitochondria, which are required to power the H^{+}/K^{+} ATPase and drive acid secretion, the quintessential parietal cell function. Of note, although mt-dsRNA accumulates in gastric epithelium when *Adar1* is deleted from parietal cells, mitochondrial gene expression is downregulated in *Adar1*-deficient parietal cells, suggesting that ADAR1 editing may promote transcription or mRNA stability of mitochondrial genes. Our results suggest that mitochondrial transcripts in parietal cells, however, are edited at a relatively low frequency by ADAR1. Taken together, it is possible that the presence alone of cytosolic mt-dsRNA, regardless of ADAR1 editing, triggers the dsRNA response, as has been previously reported.[51]

It also remains to be seen under what context(s) mt-dsRNA induces an innate immune intracellular response. Loss of *Adar1* from chief cells does not lead to an enrichment of mt-dsRNA, unlike loss of *Adar1* from parietal cells. Moreover, loss of *Adar1* from chief cells does not produce an appreciable phenotype at homeostasis, which we have previously described.[5] Finally, loss of *Adar1* from parietal

Figure 4. (***See previous page***). **Enrichment of mt-dsRNA in *Adar1*$^{\Delta PC}$ gastric epithelium.** (*A*) Following the loss of ADAR1, unedited cytosolic dsRNA is recognized by DDX58 and/or IFIH1 and leads to activation of the dsRNA response by signaling through MAVS. (*B*) Transcriptional activation of the dsRNA response in *Adar1*$^{\Delta PC}$ stomachs depends on *Mavs*. Bars represent mean ± SD fold change expression (by qRT-PCR) for dsRNA response genes from *Adar1*$^{\Delta PC}$ (*dark blue*) and *Adar1*$^{\Delta PC}$*;Mavs*$^{-/-}$ (*light blue*) gastric corpora, relative to controls (*black*), at 8 weeks of age. Each data point represents an individual mouse. Numbers of mice for each genotype are shown in parentheses. Comparisons were made by 1-way ANOVA with post-hoc Tukey tests. *$P < .0001$. Dotted line illustrates mean expression in control mice. (*C*) In *Adar1*$^{\Delta PC}$ stomachs, oxyntic atrophy and SPEM depend on signaling through MAVS. Representative confocal images of control (*top*), *Adar1*$^{\Delta PC}$ (*middle*), and *Adar1*$^{\Delta PC}$*;Mavs*$^{-/-}$ (*bottom*) stomachs at 8 weeks of age show preserved parietal cells and the absence of SPEM in *Adar1*$^{\Delta PC}$*;Mavs*$^{-/-}$ mice, similar to control mice. Scale bars, 50 μm. (*D*) dsRNA (*red*) accumulates within gastric epithelium (E-cadherin; *green*) of *Adar1*$^{\Delta PC}$*;Mavs*$^{-/-}$ mice. Scale bars, 10 μm. (*E*) Identification of dsRNA that accumulates in *Adar1*$^{\Delta PC}$*;Mavs*$^{-/-}$ stomachs. Experimental setup for immunoprecipitation and RNA-sequencing (dsRIP-seq) of dsRNA from *Adar1*-sufficient (control) and *Adar1*-deficient (*Adar1*$^{\Delta PC}$*;Mavs*$^{-/-}$) stomachs. (*F*) Table of the 10 most enriched protein-coding dsRNA in *Adar1*$^{\Delta PC}$*;Mavs*$^{-/-}$ stomachs from dsRIP-seq. Mean $\log_2$ fold changes from 3 consecutive, independent experiments are shown. Mitochondrial dsRNA is highlighted in *light blue*. FC, fold change. (*G*) Immuno-electron microscopy shows the accumulation of dsRNA within mitochondria (m) of a *Adar1*$^{\Delta PC}$*;Mavs*$^{-/-}$ parietal cell, marked by its canalicular membrane (c). A parietal cell from a control stomach (*Adar1*$^{fl/fl}$*;Mavs*$^{-/-}$) is also shown (*top*). Scale bars, 500 nm. nu, nucleus. The boxed area is magnified (*bottom right*). (*H–I*) Enrichment of dsRNA from dsRIP-seq of mouse stomachs with *Adar1*-sufficient/deficient parietal cells (*I*) or *Adar1*-sufficient/deficient chief cells (*Adar1*$^{\Delta CC}$; *I*). Mitochondrial dsRNA are marked in green. (*J*) Parietal cells from *Adar1*$^{fl/+}$*;Atp4b*^{Cre}*;Mavs*$^{-/-}$*;ROSA26*^{LSLtdTomato} (*Adar1*-sufficient) or *Adar1*$^{\Delta PC}$*;Mavs*$^{-/-}$*; ROSA26*^{LSLtdTomato} (*Adar1*-deficient) stomachs were isolated by FACS, followed by RNA processing and sequencing. Representative FACS plots (*top*) of live/dead, epithelial (EpCAM), and tdTomato (RFP) staining are shown. (*K*) Volcano plot of differential gene expression from FACS-sorted *Adar1*-sufficient or *Adar1*-deficient parietal cells reveals a relative downregulation of mitochondrial gene expression (*dark blue*) and an upregulation of metaplastic genes (*black dots* and *outlined*) in *Adar1*-deficient parietal cells (n = 3 independent experiments). Decreased/absent mitochondrial gene expression (eg, *mt-Co3*) in *Adar1*-deficient parietal cells was confirmed using RNAscope; representative confocal images are shown above the Volcano plot. RFP, red fluorescent protein; EpCAM, epithelial cell adhesion molecule.

cells leads to apoptosis and necroptosis, the latter likely through ZBP1 activation,[52,53] whereas *Adar1*-deficient chief cells are viable at homeostasis and do not undergo cell death. Whether *Adar1*-deficient parietal cell death is a direct result of mt-dsRNA signaling/editing or whether ADAR1 dictates parietal cell identity/function in RNA

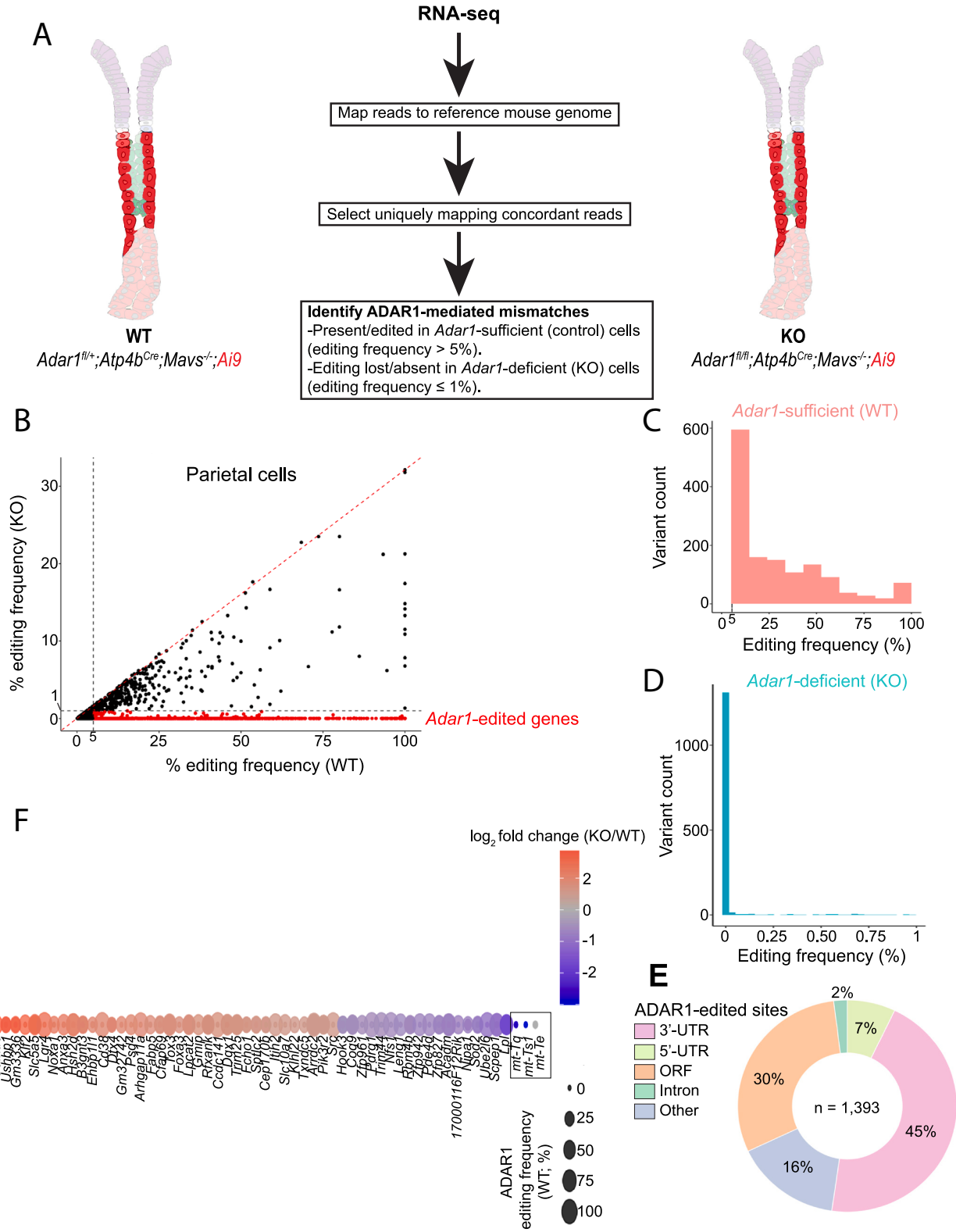

editing-dependent or editing-independent ways warrants further study.

ADAR1 editing has been proposed to promote epithelial tumorigenesis across multiple human cancers through various mechanisms.[39,54,55] For example, increased ADAR1 editing can induce coding changes in oncogenic proteins or can drive resistance to chemotherapy.[15] Our model of gastric dysplasia suggests that ADAR1 constrains the progression to gastric dysplasia: cell-specific loss of *Adar1* leads to increased expression of ISGs, upregulation of dysplastic transcripts, and transcriptional downregulation of a tumor suppressive pathway within gastric epithelium. Although this study focused on ADAR1-mediated dsRNA signaling in gastric epithelium, we would argue that the accumulation of dsRNA is not unique to the stomach and is likely relevant to extra-gastric epithelial injury. Future studies should focus on the source(s) and conserved roles for dsRNA in promoting epithelial injury and tumorigenesis.

Materials and Methods

All authors had access to the study data and have reviewed and approved this revised manuscript.

Mice

ROSA26^{LSLTdTomato} (Ai9 reporter; strain 007909), *Ifnar1*$^{-/-}$ (strain 028288), *Rag1*$^{-/-}$ (strain 002216), and *Mavs*$^{-/-}$ (strain 008634) male and female mice were obtained from the Jackson Laboratory. *Adar1*-floxed mice[19] were previously provided by Qingde Wang (University of Pittsburgh Medical Center). *Ifnlr1*$^{-/-}$ mice were kindly provided by Megan Baldridge (Washington University in St Louis School of Medicine). *Adar1*$^{\Delta CC}$ mice (*Adar1*$^{fl/fl}$;*Mist1*$^{Cre\text{-}ERT2/+}$) have been previously described and characterized.[5] All other mice used were generated in-house. Mice were maintained in a specified pathogen-free barrier facility under a 12-hour light cycle and had access to food and water ad libitum. High-dose tamoxifen (HD-Tam) treatment,[41] chronic *Helicobacter pylori* infection,[42] and characterization of *Atp4b*^{Cre};*ROSA26*^{LSLDTR} (iDTR) mice[43] have been previously described. Prior to obtaining gastric tissue, mice were euthanized using isoflurane for anesthesia, followed by cervical dislocation.

Immunohistochemistry

Mouse stomachs were excised, cut open along the lesser curvature, and pinned down in 4% paraformaldehyde for 2 hours at room temperature. Stomachs were cut into longitudinal strips and embedded in 2% low-melting agar. Paraffin-embedded sections (5 μm) were deparaffinized and rehydrated according to routine paraffin processing protocols. Endogenous peroxidase activity was quenched with 1.5% H_2O_2 in methanol for 15 minutes at room temperature. Slides were boiled in 10 mM sodium citrate buffer (pH 6.0) for 10 minutes, then blocked for 2 hours in blocking buffer (3% bovine serum albumin [BSA], 5% normal horse serum, phosphate buffered saline [PBS]) in a humidity chamber. Slides were then blocked using the Avidin/Biotin blocking kit (Vector Laboratories), according to the manufacturer's protocol. Primary antibodies used for immunohistochemistry are provided in Table 1. Signal was amplified using the VectaStain Elite ABC kit (Vector Laboratories) and developed using 3′3-diaminobenzidine tetrahydrochloride (ThermoFisher Scientific). Slides were counterstained with hematoxylin (Fisher Scientific), according to routine staining protocols. Following staining and mounting, slides were scanned using the Nanozoomer 2.0-HT (Hamamatsu), and digital files were analyzed using the NDP.2 View software (Hamamatsu).

Immunofluorescence

Mouse stomachs were excised, fixed, embedded, and deparaffinized, as described in the Immunohistochemistry section. Sections were blocked in blocking buffer (3% BSA, 1% saponin in PBS; or 5% normal donkey serum in PBS) for 2 hours at room temperature, then incubated in the appropriate primary antibody overnight at 4°C in a humidity chamber. Information related to the primary and secondary antibodies used for immunofluorescent staining is provided in Table 1. Following secondary antibody staining and washing, sections were mounted in 4',6-diamidino-2-phenylindole (DAPI) Fluoromount-G (Southern Biotech) or incubated in Hoescht 33258 (1:20,000) for 2 minutes at room temperature and mounted using ProLong Gold antifade reagent (Invitrogen). Images were obtained using the Olympus FV1200 confocal microscope, and *Z*-stacks were reconstructed into images using Amaris software (Thermo Fisher Scientific).

Isolation of Parietal Cells

Mouse stomachs were excised and cut open along the lesser curvature. The forestomach and antrum were discarded. The remaining corpus was minced and incubated in 10 mL of digest buffer (20 mM HEPES, 0.2% BSA, 1% penicillin-streptomycin, 50 ug/mL gentamicin, 1 mg/mL

Figure 5. (***See previous page***). **Characterization of the ADAR1 editome in parietal cells.** (*A*) Schematic of RNA-seq analysis pipeline to identify ADAR1-edited sites (see Methods for details). (*B*) Editing frequencies for *Adar1*-sufficient (WT) and *Adar1*-deficient (KO) parietal cells. *Dotted black lines* represent established cutoffs for ADAR1 editing frequency in WT cells (5%) and KO cells (1%). ADAR1-edited sites meeting the established cutoff requirements are shown in red. *Dotted red line* denotes equal ADAR1 editing between WT and KO samples. (*C–D*) Distribution of ADAR1 editing frequencies in parietal cells. Note that the editing frequency for nearly all ADAR1-edited sites (*C*) is absent in *Adar1*-deficient (KO) cells (*D*). (*E*) Gene locations for ADAR1-edited sites in parietal cells. UTR, untranslated region. ORF, open reading frame. "Other" refers to intergenic, upstream, or downstream regions. (*F*) Correlation between gene expression and ADAR1 editing among the most highly ADAR1-edited genes in parietal cells. Note that differentially expressed mitochondrial genes (outlined; *mt-Tq*, *mt-Ts1*, *mt-Te*) are not significantly edited by ADAR1.

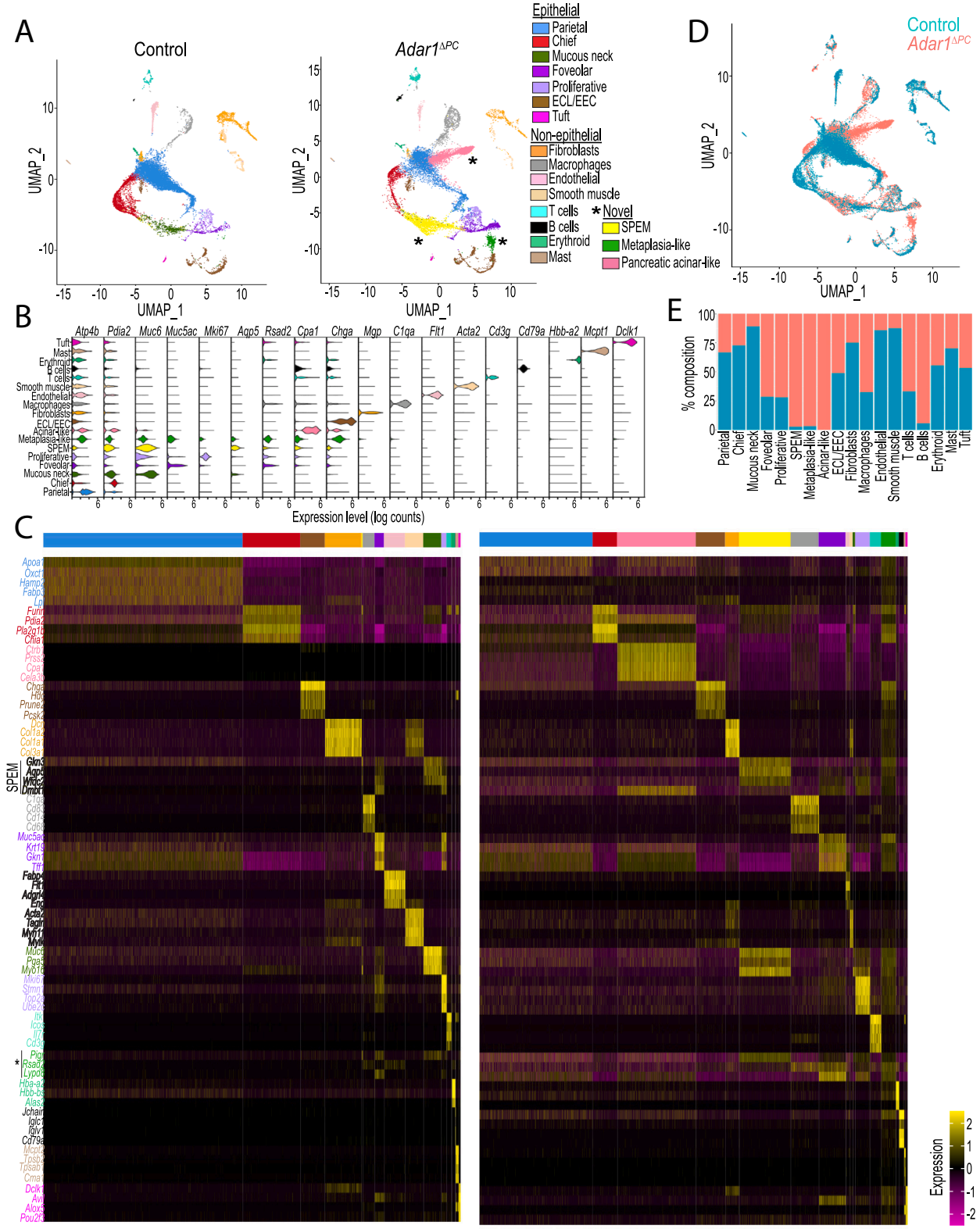

Figure 6. Transcriptional profiling of the *Adar1*$^{\Delta PC}$ gastric environment. (*A*) scRNA-seq profiles of control (*left*) and *Adar1*$^{\Delta PC}$ (*right*) gastric corpora at 8 weeks of age. Populations unique to *Adar1*$^{\Delta PC}$ stomachs are highlighted by an asterisk (*). Profiles were generated from single cells pooled from 3 mice per genotype. EEC, enteroendocrine cells. (*B*) Violin plots showing expression of characteristic markers in each of the cell populations of *Adar1*$^{\Delta PC}$ stomachs. (*C*) Heat map of gene expression for gastric epithelial and nonepithelial populations in control (*left*) and *Adar1*$^{\Delta PC}$ (*right*) stomachs at 8 weeks of age. Cell-specific markers are color-coded (see legend in *A*). * denotes metaplasia-like population. (*D–E*) Superimposed scRNA-seq profiles of control (*aqua*) and *Adar1*$^{\Delta PC}$ stomachs (*orange*; *D*), with the census for each cell population normalized to cell counts (*E*).

collagenase, and DMEM) for 30 minutes at 37°C with periodic pipetting. Cells were centrifuged at 800 rpm for 5 minutes at room temperature. Supernatant was removed, and the cell pellet was washed with 10 mL of wash buffer (50 ug/mL gentamicin, 1% penicillin-streptomycin, 0.5 mM dithiothreitol [DTT], and Dulbecco's Modified Eagle's

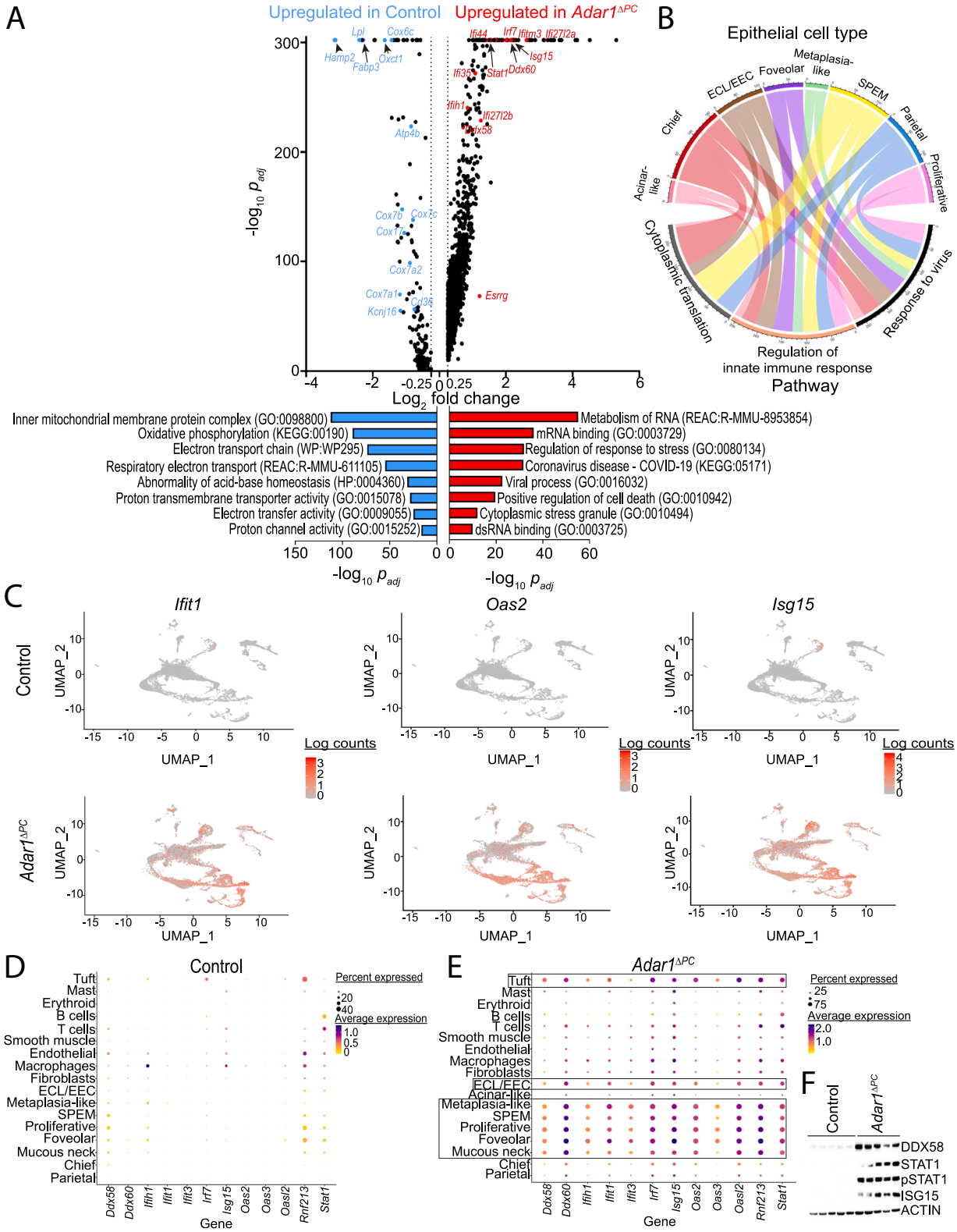

Medium [DMEM]/F12 Ham). Cells were centrifuged at 800 rpm for 5 minutes at room temperature. The cell pellet was washed and centrifuged once more. Cells were washed twice with sorting buffer (DPBS, 25mM HEPES, 0.5 mM EDTA) and resuspended in 100 μL of e780 Live/Dead stain (Invitrogen) for 7 minutes on ice. Fifty μL of Fc blocking agent (made in-house) were added, and cells were incubated for an additional 7 minutes. Cells were washed twice with sorting buffer, resuspended in 100 μL of sorting buffer containing anti-EpCAM BV421 antibody (Biolegend), and incubated on ice for 20 minutes, then washed twice with sorting buffer. Cells were then filtered through a 100-μm filter and sorted on the BD FACS Aria Fusion (Becton Dickinson) for live EpCAM$^+$ cells that were either positive or negative for the Ai9 reporter (tdTomato/RFP). RNA was isolated from sorted RFP$^+$ and RFP$^-$ epithelial cells, using the RNeasy Plus Mini Kit (Qiagen), according to the manufacturer's protocol.

RNAscope

Mouse stomachs were excised, fixed, embedded, and sectioned as described in the Immunohistochemistry section. Sections were processed and stained according to the manufacturer's protocol for the RNAscope Multiplex Fluorescent Reagent Kit v2 (Advanced Cell Diagnostics), with some modifications. Sections were deparaffinized with Histoclear (National Diagnostics) instead of xylene. Antigen retrieval was performed with 10 mM sodium citrate buffer (pH 6.0) in a pressure cooker for 3 minutes. Sections were incubated in RNAscope Protease Plus for 15 minutes at 40°C. All 40°C incubation steps were carried out in a humidified chamber placed in a Model 10 Lab Oven (Quincy Lab, Inc). Following protease treatment, slides were stored overnight at room temperature in 5× saline sodium citrate (SSC) buffer. Information related to the probes and fluorophores used for RNAscope is provided in Table 1.

Histologic Scoring

For scoring of tdTomato/parietal cell staining, 4 random high-powered fields (20× magnification) were selected from 3 to 5 mice per genotype. For Ki-67 scoring, the number of Ki-67-positive cells per 20× high-powered field was counted for each mouse. For TROP2 scoring, 2 to 4 gastric strips were counted from 4 to 5 mice per genotype. All histologic scoring was performed by an investigator blinded to the mouse genotypes.

Bulk RNA-seq

Mouse stomachs from control or *Adar1*$^{\Delta PC}$ stomachs at the indicated developmental stages were excised and processed for RNA isolation using the Qiagen RNeasy Mini Kit, per the manufacturer's instructions. For E17.5 and P1 stomachs, the forestomach was discarded, and the glandular stomach was used. For P15, only gastric corpus sections were processed. Samples were indexed, pooled, and sequenced on an Illumina NovaSeq 6000. Basecalls and demultiplexing were performed with Illumina's bcl2fastq software and a custom python demultiplexing program with a maximum of one mismatch in the indexing read. RNA-seq reads were then aligned to the Ensembl release 76 primary assembly with STAR version 2.7.9a.[56] Gene counts were derived from the number of uniquely aligned unambiguous reads by Subread:featureCount version 2.0.3.[57] Isoform expression of known Ensembl transcripts were quantified with Salmon version 1.5.2.[58] Sequencing performance was assessed for the total number of aligned reads, total number of uniquely aligned reads, and features detected. All gene counts were then imported into the R/Bioconductor package EdgeR,[59] and TMM normalization size factors were calculated to adjust for samples with differences in library size. Ribosomal genes and genes not expressed in the smallest group size (minus one) samples greater than one count-per-million were excluded from further analysis. The TMM size factors and the matrix of counts were then imported into the R/Bioconductor package Limma.[60] Weighted likelihoods based on the observed mean-variance relationship of every gene and sample were then calculated, and the count matrix was transformed to moderated $\log_2$ counts-per-million with Limma's voomWithQualityWeights.[61] The performance of all genes was assessed with plots of the residual standard deviation of every gene to their average log-count with a robustly fitted trend line of the residuals. Differential expression analysis was then performed to analyze for differences between conditions, and the results were filtered for only those genes with Benjamini-Hochberg false-discovery rate adjusted P values less than or equal to .05.

scRNA-seq Analyses

Isolation, processing, and library construction for scRNA-seq from gastric corpus mucosa were performed, using the Chromium Next GEM Single Cell 3' Kit v3.1 (10X Genomics), as previously described.[62] The above filtered h5 count matrices were imported into R environment and were analyzed by the Seurat (v4.3.0) package. The count matrices were further filtered to exclude cells with

Figure 7. (***See previous page***). **Loss of *Adar1* from parietal cells leads to a glandular dsRNA response.** (*A*) Differential expression analyses of *Adar1*-sufficient (control; *left*) and *Adar1*-deficient (*Adar1*$^{\Delta PC}$; *right*) parietal cells from scRNA-seq profiles show increased expression of multiple dsRNA response transcripts (*red*) in *Adar1*-deficient parietal cells. Pathway analyses (*bottom*) were performed using g:Profiler.[20] (*B*) Circos plot of the most upregulated transcriptional pathways across gastric corpus epithelial populations in *Adar1*$^{\Delta PC}$ mice. (*C*) Dim plots show activation of the dsRNA response across multiple gastric epithelial lineages in *Adar1*$^{\Delta PC}$ mice (*bottom*). (*D–E*) Dot plots demonstrate transcriptional upregulation of dsRNA response genes across multiple gastric epithelial lineages (outlined) in *Adar1*$^{\Delta PC}$ (*E*) but not in control (*D*) mice at 8 weeks of age. EEC, enteroendocrine cells. (*F*) The dsRNA response is activated in *Adar1*$^{\Delta PC}$ stomachs. Each lane of the Western blot corresponds to gastric corpus tissue from an individual mouse at 8 weeks of age. pSTAT1, phospho-STAT1.

mitochondrial percent ≥ median+3*(median of absolute deviations), and those with high gene counts defined by spline regression method. The filtered and adjusted counts for each sample were normalized with the SCTransform (v2) function. After scaling the data, principal component analysis (PCA) was performed to reduce the data to top 25

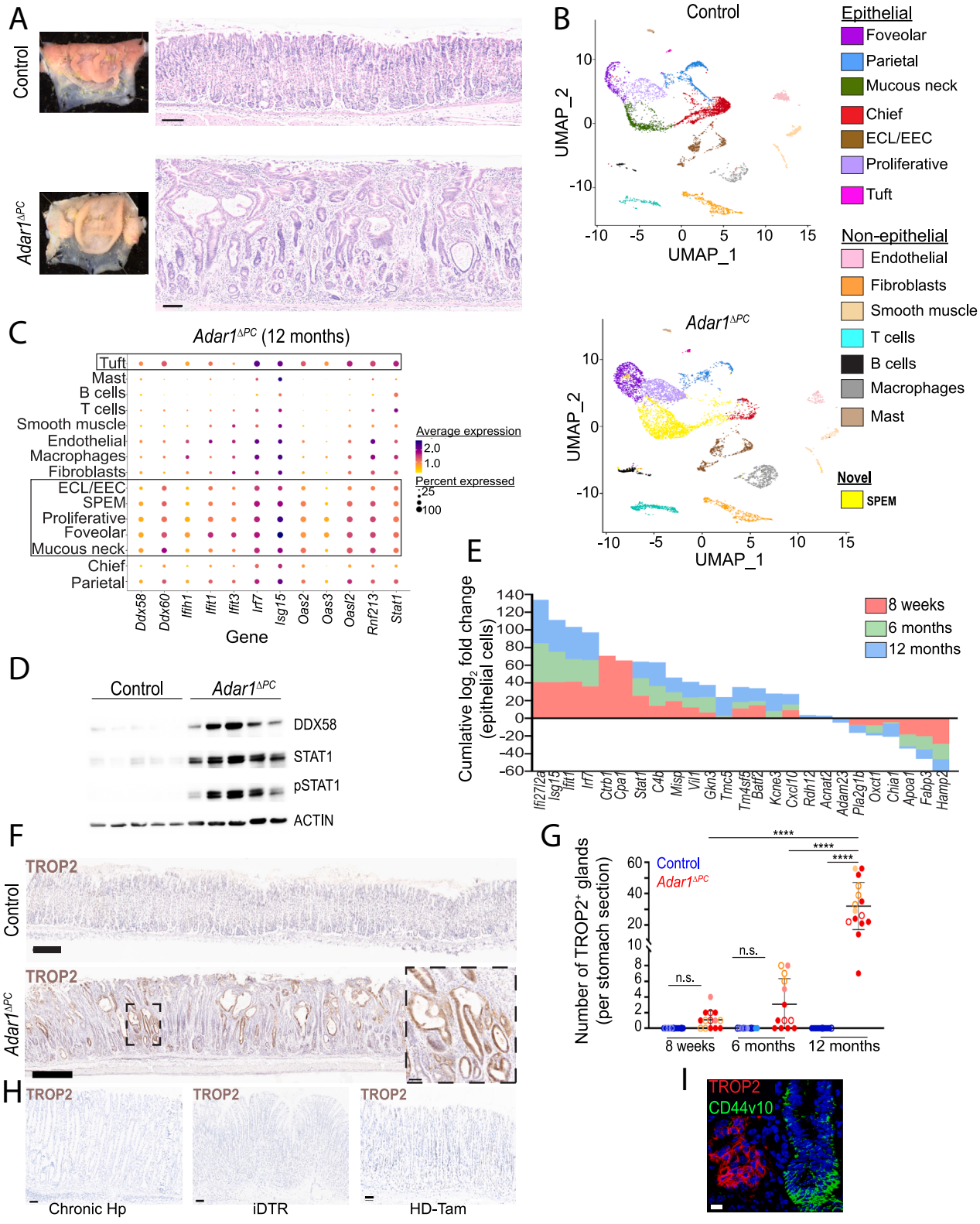

PCA components. Cells were then clustered with the Louvain algorithm at a 0.3 resolution, and data dimensional reduction was performed with the Uniform Manifold Approximation and Projection (UMAP) method. Markers for each cell cluster were generated by using Wilcoxon rank sum tests in the FindAllMarkers function, and cluster identities were defined by known marker genes for gastric epithelial and nonepithelial cells. Differential expression between *Adar1*$^{\Delta PC}$ and control mice were tested by the same Wilcoxon statistics in the FindMarkers function, and dysregulated genes were determined by Benjamini-Hochberg with adjusted P values $< .05$. To cross-reference our data to human gastric cancer, human stomach RNA-seq data set from the TCGA STAD project[47] was analyzed to determine differential expressed genes in human gastric adenocarcinoma with different molecular subtypes. First, gene count data were imported into the R environment by package EdgeR,[59] and TMM normalization size factors were calculated to adjust samples for differences in library size. Ribosomal genes and genes with count-per-million (CPM) ≥ 1 in less than 10% of all samples were excluded from further analysis. The TMM size factors and the matrix of counts were then imported into the R package limma.[60] Weighted likelihoods based on the observed mean-variance relationship of every gene and sample were then calculated for all samples with the voomWithQualityWeights function[61] and were fitted using a limma generalized linear model. Differential expression analysis was then performed to analyze differences between a subtype and the normal gastric tissue, and DEGs were defined for those genes with absolute fold change ≥ 2 at Benjamini-Hochberg adjusted P values $< .05$.

qRT-PCR

RNA was extracted using the RNeasy Mini Kit (Qiagen), per the manufacturer's instructions. RNA was converted to cDNA using the PrimeScript cDNA synthesis kit (Takara). qRT-PCR was performed using Fast SYBR Green Master Mix (Applied Biosystems) on the QuantStudio 3 instrument (Applied Biosystems). Primer sequences are provided in Table 1.

Western Blotting

Mouse gastric corpus tissue was snap-frozen in liquid nitrogen and stored at −80°C until further use. Tissue was thawed in cold RIPA buffer containing protease/phosphatase inhibitor cocktail (Thermo Scientific), then sonicated 3 times on ice. Lysates were centrifuged at 21,130 *g* for 30 minutes at 4°C, and protein concentrations were determined using the BCA Protein Assay Kit (Pierce). Protein loading, transfer to a nitrocellulose membrane, and antibody probing have been previously described.[5] Information related to the antibodies used for Western blotting is provided in Table 1. Original Western blots are provided as Supplemental Western Blots.

Flow Cytometry

To obtain gastric cells, stomachs were dissected and washed with PBS. The forestomach was removed, and the gastric corpus mucosa was cut into small pieces. Gastric tissue was digested with 100 U/mL of collagenase IV (Sigma-Aldrich), then passed through a 100-μm filter to obtain a single-cell suspension. Prior to staining, cells were quantified using a hemocytometer. Cells were first stained with 50 to 100 μL of a 1:1000 Viability dye solution (Invitrogen Fixable Viability Dye eFluor 506 or Fixable Viability Dye eFluor 780, eBioscience) in PBS for 30 minutes at 4°C. This was followed by blocking with 100 μg of 2.4G Fc blocking agent (made in-house) for 20 minutes at 4°C. Cells were then stained with surface antibodies (see Table 1) in FACS buffer at 4°C for 1 hour. Following surface staining, fixation and permeabilization were performed using the Foxp3/Transcription Factor Staining Buffer Set (eBioscience) at room temperature for 30 minutes. Intracellular staining was performed overnight at 4°C with 10% permeabilization buffer and 90% FACS buffer. After staining, cells were resuspended in FACS buffer and passed through a 100-μm filter before flow cytometric analysis using a FACSCanto (BD Biosciences). Analyses were performed using FlowJo v10 (TreeStar).

dsRNA immunoprecipitation (dsRIP)

Mouse stomachs were excised and cut open along the lesser curvature. RNA from the gastric corpus was isolated

Figure 8. (***See previous page***). **A sustained dsRNA response leads to gastric dysplasia in *Adar1*$^{\Delta PC}$ mice.** (*A*) Compared with age-matched controls (*top*), *Adar1*$^{\Delta PC}$ stomachs show significant glandular distortion at 12 months of age. Scale bars, 200 μm. Gross morphologic images are also shown (*left*). (*B*) scRNA-seq profiles of control (*top*) and *Adar1*$^{\Delta PC}$ (*bottom*) gastric corpora at 12 months of age. Profiles were generated from single cells pooled from three mice per genotype. (*C*) Dot plots show a sustained transcriptional upregulation of the dsRNA response across multiple gastric epithelial lineages (*outlined*) in *Adar1*$^{\Delta PC}$ mice at 12 months of age. (*D*) The dsRNA response remains activated in *Adar1*$^{\Delta PC}$ stomachs. Each lane of the Western blot corresponds to gastric corpus tissue from an individual mouse at 12 months of age. pSTAT1, phospho-STAT1. (*E*) Waterfall plot shows cumulative fold changes within *Adar1*$^{\Delta PC}$ corpus gastric epithelium (relative to age-matched controls) at various time points for select transcripts. (*F*) By 12 months of age, *Adar1*$^{\Delta PC}$ stomachs (*bottom*) express the dysplastic marker, TROP2[40] (*brown*), which is absent from age-matched control stomachs (*top*). Scale bars, 200 μm. Magnified boxed area is shown (scale bar, 50 μm). (*G*) The extent of gastric dysplasia increases over time in *Adar1*$^{\Delta PC}$ mice. The number of TROP2-positive gastric glands (mean ± SEM) were counted from 2 to 4 gastric strips per mouse at each indicated age. Each color corresponds to a different mouse. Quantification of 4 to 5 mice per genotype was performed by an investigator blinded to the genotypes. Comparisons were done by 1-way ANOVA with post-hoc Tukey tests. ****$P < .0001$; n.s., not significant ($P > .05$). (*H*) TROP2 expression is not seen in other validated models of oxyntic atrophy and SPEM, including *Helicobacter pylori* infection (Hp; *left*),[42] *Diphtheria* toxin-inducible ablation of parietal cells using *Atp4b*^{Cre}; *ROSA26*^{LSLDTR} mice[43] (iDTR; *middle*), or acute injury with HD-Tam[41] (*right*). Scale bars, 50 μm. (*I*) CD44v10 (*green*) and TROP2 (*red*) expression in a representative *Adar1*$^{\Delta PC}$ stomach at 12 months. Scale bar, 10 μm. For (*B*) and (*C*): EEC, enteroendocrine cells.

using the RNeasy Plus Mini Kit (Qiagen), according to the manufacturer's protocol. Approximately 4.5 μg of RNA were set aside as the total input. The remaining RNA was divided into 2 equal halves, one for immunoprecipitation with the K1 antibody (Exalpha Biologicals), the other using the IgG control (Sigma). For immunoprecipitation, 10 μg of

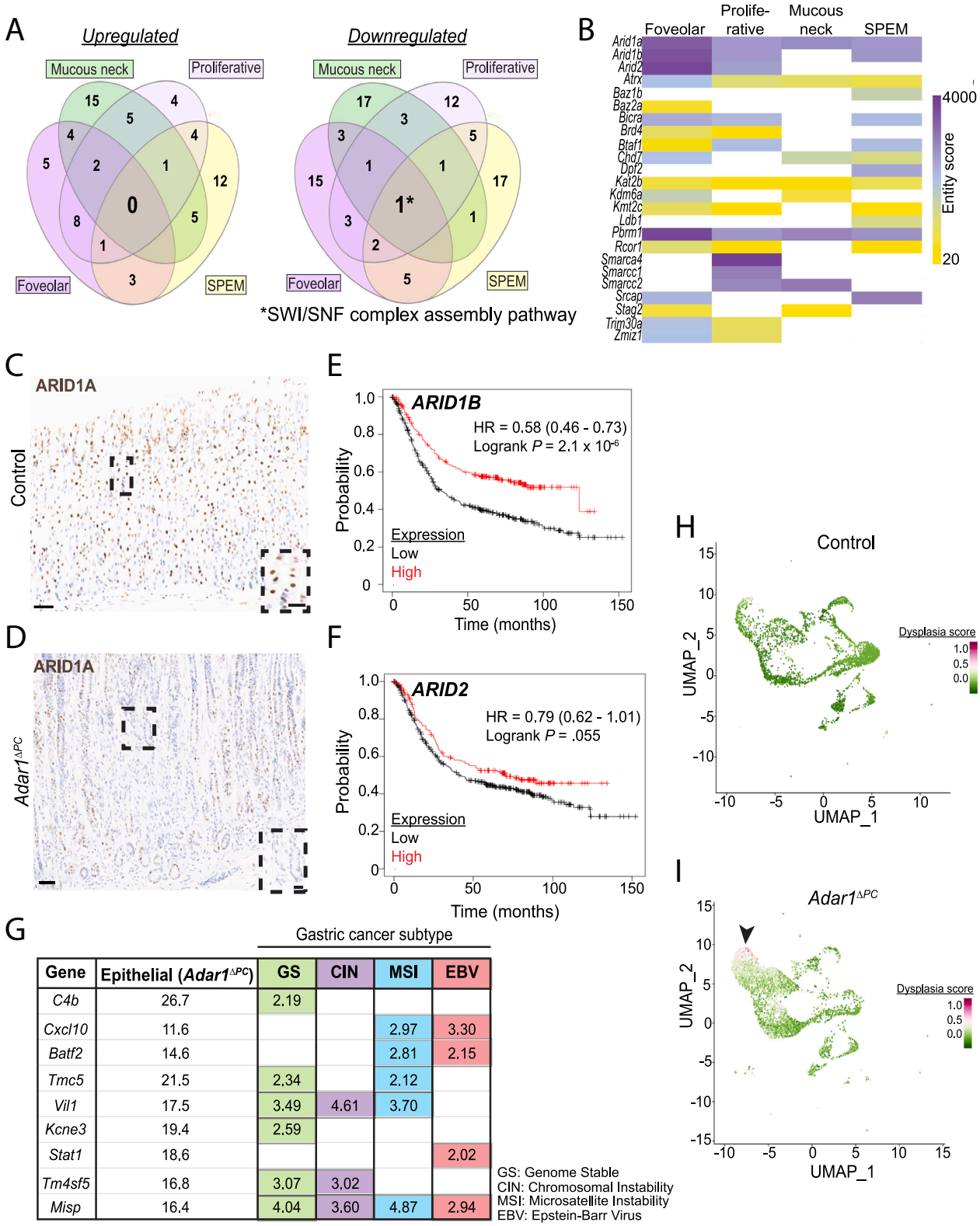

G

Gene	Epithelial (*Adar1*$^{\Delta PC}$)	Gastric cancer subtype: GS	CIN	MSI	EBV
C4b	26.7	2.19			
Cxcl10	11.6			2.97	3.30
Batf2	14.6			2.81	2.15
Tmc5	21.5	2.34		2.12	
Vil1	17.5	3.49	4.61	3.70	
Kcne3	19.4	2.59			
Stat1	18.6				2.02
Tm4sf5	16.8	3.07	3.02		
Misp	16.4	4.04	3.60	4.87	2.94

GS: Genome Stable
CIN: Chromosomal Instability
MSI: Microsatellite Instability
EBV: Epstein-Barr Virus

K1 (2.5 μg/μL) or mouse IgG (1 μg/μL) antibody was added to isolated RNA in dsRIP buffer (100 mM NaCl, 50 mM Tris-HCl, pH 7.5, 3 mM $MgCl_2$, 0.5% IGEPAL CA-630, 1× protease inhibitor cocktail [Thermo Scientific], 40 units/mL SUPERase-In RNase Inhibitor [Invitrogen], and RNase-free water) and rotated overnight at 4°C. The next day, RNA-antibody complexes were incubated with Protein G Dynabeads (Invitrogen) pre-washed in dsRIP buffer and rotated for 1 hour at 4°C. Tubes were placed on a magnetic rack to collect the beads, and supernatants were collected as the unbound fraction. Beads were washed 4 times with dsRIP buffer at 4°C. To elute immunoprecipitated dsRNA, 1 mL TRIzol reagent (Invitrogen) was added to both the beads and the unbound fraction. Samples were vortexed and incubated for 5 minutes at room temperature. 200 μL of chloroform were added, prior to mixing the samples by hand for 15 seconds and incubating for 3 minutes at room temperature. Samples were spun at 13,000 *g* for 15 minutes at 4°C. The aqueous phase was carefully removed, and 200 μL of chloroform were added. Samples were shaken by hand for 15 seconds, incubated on ice for 5 minutes, and spun at 13,000 *g* for 15 minutes at 4°C. Fifteen μg of RNase-free glycogen (Thermo Scientific) were added before gently tapping the tubes to mix. 100% isopropanol was added to each tube, and the samples were kept at −20°C overnight. The next day, samples were centrifuged at 13,000 *g* for 10 minutes at 4°C. The supernatant was discarded, and 1 mL of 75% ethanol in RNase-free water was added to the pellet. Samples were centrifuged at 8000 *g* for 5 minutes at 4°C, the supernatant was discarded, and the pellet was allowed to air dry at room temperature for 5 to 10 minutes. Pellets were resuspended in RNase-free water and submitted for RNA sequencing.

Differential Expression Analysis for dsRIP

Differential expression analyses of dsRIP between *Adar1*-sufficient and -deficient parietal cells and chief cells were adapted from a previous protocol.[63] Specifically, the sequencing reads from dsRIP were first processed by adapter trimming using TrimGalore (version 0.6.0). Trimmed reads were then aligned to the GENCODE Release M32 (GRCm39) genome using STAR (version 2.5.1a) with default parameters. Gene read counts were obtained using the STAR quantMode module (–quantMode GeneCounts) with GENCODE M32 transcript annotation. Only unique mappers were included in the gene read counts. For differential expression, only genes with at least 10 raw reads in all of the replicates of at least 1 condition were included in subsequent analyses. To identify genes with significant differential expression between *Adar1*-sufficient and -deficient samples, we utilized differential read count analysis using generalized linear models implemented in edgeR (glmQLFTest function) by first normalizing the gene read count of each sample using the TMM method implemented in the edgeR package, followed by contrasting the *Adar1*-deficient sample (Adar1-KO) against the *Adar1*-sufficient (control) sample, after normalization to their respective input samples in $\log_2$-transformed values $((dsRIP_{Adar1\text{-}KO} - Input_{Adar1\text{-}KO}) - (dsRIP_{Control} - Input_{control}))$. We determined genes to be upregulated or downregulated based on whether the $\log_2$ fold change in gene read counts in the Adar1-KO sample was greater than 1 or less than −1, respectively, in comparison to the control sample with an adjusted P value $< .05$.

Immuno-electron Microscopy

For immunolocalization at the ultrastructural level, mouse stomachs were excised and fixed in 4% paraformaldehyde/0.025% glutaraldehyde (Polysciences) in 100 mM PIPES/0.5 mM $MgCl_2$ (pH 7.2) for 1.5 hours at 4°C. Samples were then embedded in 10% gelatin and infiltrated overnight with 2.3 M sucrose/20% polyvinyl pyrrolidone in PIPES/$MgCl_2$ at 4°C. Samples were trimmed, frozen in liquid nitrogen, and sectioned with a Leica Ultracut UCT7 cryo-ultramicrotome (Leica Microsystems). Ultrathin sections of 65 nm were blocked with 5% fetal bovine serum (FBS)/5% goat serum for 30 minutes and subsequently incubated with mouse anti-dsRNA K1 antibody (1:25) for 1 hour at room temperature. Following washes in blocking buffer, sections were incubated with secondary anti-mouse IgG (H+L) antibody conjugated to 12 nm colloidal gold (Jackson ImmunoResearch Laboratories) for 1 hour. Sections were stained with 0.3% uranyl acetate/2% methyl cellulose and viewed on a JEOL 1200 EX transmission electron microscope (JEOL USA) equipped with an AMT 8-megapixel digital camera and AMT Image Capture Engine V602 software (Advanced

Figure 9. (***See previous page***). **Gastric dysplasia in *Adar1*$^{\Delta PC}$ mice bears transcriptional similarities to human gastric adenocarcinoma.** (*A*) Venn diagram of CompBio-enriched pathways[45] that are either upregulated (*left*) or downregulated (*right*) across four distinct epithelial lineages in *Adar1*$^{\Delta PC}$ stomachs at 12 months of age, relative to 8 weeks of age. The SWI/SNF complex assembly pathway (*) was identified as the sole pathway downregulated across multiple gastric epithelial lineages in *Adar1*$^{\Delta PC}$ stomachs at 12 months of age. (*B*) Heat map based on CompBio-calculated Entity scores for genes associated with the SWI/SNF complex assembly pathway across gastric epithelial lineages. (*C–D*) ARID1A (*brown*) expression in control (*C*) and *Adar1*$^{\Delta PC}$ stomachs (*D*) at 12 months of age. Boxed areas are magnified. Scale bars, 50 μm and 20 μm (*inset*). (*E–F*) Kaplan-Meier survival curves for human gastric cancer based on select genes associated with the SWI/SNF complex assembly pathway (*B*), using the Kaplan-Meier plotter.[46] HRs, with 95% confidence intervals in parentheses, along with log-rank *P* values, are provided. (*G*) Epithelial expression of select genes from *Adar1*$^{\Delta PC}$ stomachs at 12 months of age (see Methods) were cross-referenced to gene expression in human gastric cancer molecular subtypes.[31] For *Adar1*$^{\Delta PC}$, data represent linear fold change in epithelial expression, relative to age-matched controls. (*H–I*) A dysplasia signature score, based on genes identified in (*G*), was mapped onto scRNA-seq profiles from control (*H*) and *Adar1*$^{\Delta PC}$ (*I*) stomachs at 12 months of age. Dysplastic genes associated with human gastric adenocarcinoma are expressed in a cellular subset in *Adar1*$^{\Delta PC}$ stomachs at 12 months of age (*I*; *arrowhead*).

Microscopy Techniques). All labeling experiments were conducted in parallel with controls omitting the primary antibody.

ADAR1-dependent Variant Calling

To identify ADAR1-dependent modifications, variants were called on the aligned RNA reads using freebayes

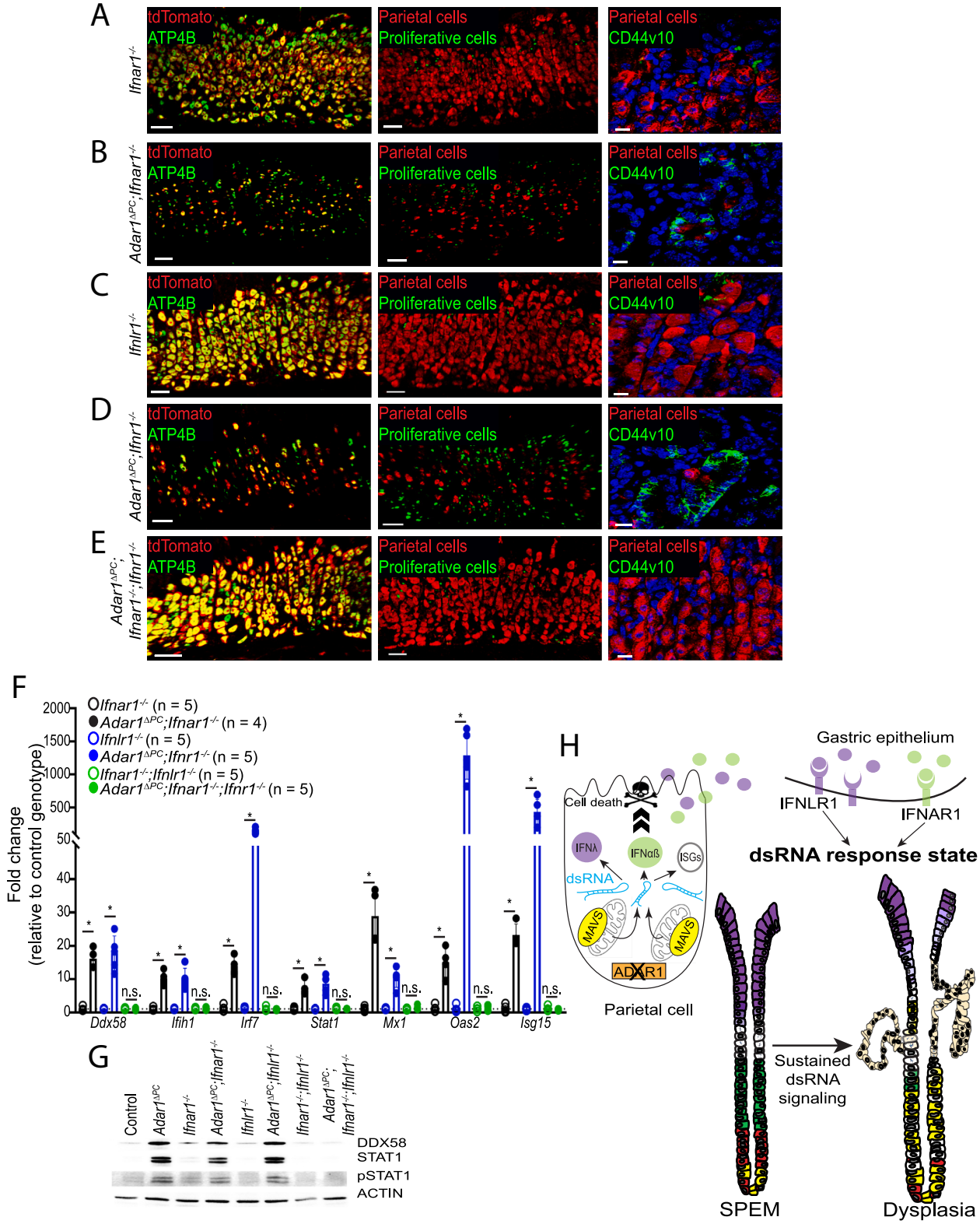

Table 1. Reagents and Resources

Reagent or resource	Source	Identifier
Antibodies (immunofluorescence; immunohistochemistry)		
Anti-mCherry, goat	Origene	AB0081-200
Anti-ATP4B, rabbit	Abcam	AB176992
Phalloidin-647	Invitrogen	A22287
Anti-E-Cadherin (24E10), rabbit	Cell signaling	3195
Hoechst 33258	Thermo Fisher Scientific	H3569
DAPI Fluoromount-G	Southern Biotech	0100-20
Anti-Gastric Intrinsic Factor (GIF), rabbit	David Alpers (Washington University School of Medicine)	N/A
Griffonia simplicifolia (GSII)-488	Invitrogen	L21415
Anti-Ki-67, rabbit	Abcam	ab15580
Anti-TROP2, goat	R&D Systems	AF1122
Anti-ARID1A, rabbit	Cell signaling	12354S
Anti-Phospho-MLKL, rabbit	Abcam	ab196436
K1 anti-dsRNA, mouse	Exalpha/SCICONS	10020200
Donkey anti-rabbit IgG, AF-488	Invitrogen	A32790
Donkey anti-mouse IgG, AF-594	Invitrogen	A10037
Donkey anti-rat IgG, AF-488	Invitrogen	A21208
CD44v10-e16, rat	Cosmo Bio USA	LKG-M002
Horse anti-goat IgG (H+L), biotinylated	Vector Laboratories	BA-9500-1.5
Horse anti-rabbit IgG (H+L), biotinylated	Vector Laboratories	BA-1100
Antibodies (Western blot)		
Anti-Rig-I (D14G6) (DDX58), rabbit	Cell Signaling Technologies	3743
Anti-STAT1, rabbit	Cell Signaling Technologies	9172
Anti-Phospho-STAT1 (Y701), rabbit	Cell Signaling Technologies	9167
Anti-ISG15, mouse	Santa Cruz	sc-166755
Anti-β-Actin, mouse	Sigma	A5441
Cleaved-CASPASE 3, rabbit	Cell Signaling Technologies	9664
Anti-rabbit-HRP	Cell Signaling Technologies	7074
Anti-mouse-HRP	Santa Cruz	sc-516102
Antibodies (flow cytometry)		
PD-1 PE-Cyanine7 (clone J43)	eBioscience	25-9985-82
CD69 Alexa Fluor 700 (clone H1.2F3)	eBioscience	56-0691-80
CD45 Alexa Fluor™ 700 (clone 30-F11)	eBioscience	56-0451
CD19 BV650 (clone 6D5)	Biolegend	115541
NK1.1 BV650 (clone PK136)	BD Bioscience	108736
TCRgd BV650 (clone B1)	BD Bioscience	564156
CD4 eFluor 506 (clone RM4-5)	Biolegend	69-0042-82
CD8a PE-eFluor610 (clone 53-6.7)	eBioscience	61-0081-82
IFN-gamma eF450 (clone MXG1.2)	eBioscience	501124215
IL-17A (PE; clone eBio17B7)	eBioscience	12-7177-81
IL-4 (AF488; clone 11B11)	eBioscience	53-7041-82
Foxp3 (PerCP-Cyanine5.5; clone FJK-16s)	eBioscience	45-5773-82
RNAScope		
Mm-mt-Co3-C1	Advanced Cell Diagnostics	1147431-C1
Mm-Atp4b-C2	Advanced Cell Diagnostics	462781-C2

Figure 10. (***See previous page***). **The dsRNA response state in *Adar1*$^{\Delta PC}$ stomachs depends on both type I and type III IFN signaling.** (*A–E*) Oxyntic atrophy (*left*) and characteristic SPEM changes (*middle*, *right*) in *Adar1*$^{\Delta PC}$ mice are independent of either type I IFN signaling through the IFNAR1 receptor (*A–B*) or of type III IFN signaling through the IFNLR1 receptor (*C–D*). However, *Adar1*$^{\Delta PC}$ mice deficient in both type I and type III IFN signaling are completely protected from oxyntic atrophy and from SPEM (*E*). (*F–G*) Activation of the dsRNA response is unaffected by loss of either type I or type III IFN signaling alone, but the combined loss of type I and type III IFN signaling completely blocks the dsRNA response at the transcriptional (*F*) and protein (*G*) levels. In (*F*), bars represent mean ± SD fold change expression (by qRT-PCR) for dsRNA response genes, relative to their corresponding control genotypes, from gastric corpora at 8 weeks of age. Each data point represents an individual mouse. The number of mice per genotype is shown in parentheses. Comparisons were made by 1-way ANOVA with post-hoc Tukey tests. *$P < .0001$; n.s., not significant ($P > .05$). In (*G*), each lane of the Western blot is a gastric corpus section from a representative mouse from each genotype, at 8 weeks of age. pSTAT1, phospho-STAT1. (*H*) Loss of *Adar1* from gastric parietal cells triggers the accumulation of mt-dsRNA and a glandular dsRNA response state that depends on both type I (IFN$\alpha\beta$) and type III (IFNλ) signaling. Sustained dsRNA signaling promotes the development of gastric pre-neoplastic lesions.

Table 1. Continued

Reagent or resource	Source	Identifier
RNAscope Multiplex Fluorescent Reagent Kit v2	Advanced Cell Diagnostics	323110
Commercial assays		
In Situ Cell Death Detection Kit, Fluorescein (TUNEL)	Roche	11684795910
Dynabeads Protein G	Invitrogen	10003D
DAB Substrate Kit	ThermoFisher	34065
Avidin/Biotin blocking Kit	Vector Laboratories	SP-2001
VECTASTAIN Elite ABC Kit, Peroxidase	Vector Laboratories	PK-6100
RNeasy Mini Kit	Qiagen	74104
RNeasy Plus Mini Kit	Qiagen	74134
DNase Set	Qiagen	79254
Prime Script RT Reaget Kit (Perfect Real Time)	Takara	RR037A
Fast SYBR Green Master Mix	Applied Biosystems	4385612
Pierce BCA Protein Assay Kit	Thermo Scientific	23227
Oligonucleotides	Forward	Reverse
Ddx58	5′-GCAGAACTGGAACAGGTCGT -3′	5′ -TGTTCGAAGTCCGGGATG - 3′
Ifih1	5′ -TGATGCACTATTCCAAGAACTAACA - 3′	5′ - TCTGTGAGACGAGTTAGCCAAG- 3′
Irf7	5′ -GAGACTGGCTATTGGGGGAG - 3′	5′ -GACCGAAATGCTTCCAGGG - 3′
Stat1	5′ -CGCGCATGCAACTGGCATATAACT - 3′	5′ - AAGCTCGAACCACTGTGACATCCT- 3′
Mx1	5′ - TCTGAGGAGAGCCAGACGAT- 3′	5′ -ACTCTGGTCCCCAATGACAG - 3′
Oas2	5′ -TAGACCAGGCCGTGGATG - 3′	5′ -GTTTCCCGGCCATAGGAG - 3′
Isg15	5′ -GGAACGAAAGGGGCCACAGCA - 3′	5′ -CCTCCATGGGCCTTCCCTCGA - 3′
Gapdh	5′ -AGCTTGTCATCAACGGGAAG - 3′	5′ -TTTGATGTTAGTGGGGTCTCG - 3′
Chemicals, peptides, and recombinant proteins		
NuPAGE MOPS Running Buffer (20X)	Invitrogen	NP0001
NuPAGE Transfer Buffer (20X)	Invitrogen	NP0006
NuPAGE Sample Reducing Agent	Invitrogen	NP0004
NuPAGE Antioxidant	Invitrogen	NP0005
NuPAGE LDS Sample Buffer (4X)	Invitrogen	NP0007
HALT Protease/ Phosphatase inhibitor cocktail	Thermo Scientific	78443
SuperSignal West Pico Chemilluminescent Substrate	ThermoFisher	34577
NuPAGE 4-12% Bis-Tris gels	Invitrogen	NP0322BOX
Hematoxylin	Fisher HealthCare	220-100
Histo-Clear	National Diagnostics	HS-200
Collagenase, Type IA from *Clostridium histolyticum*	MilliporeSigma	C9891
Experimental models: organisms/strains		
C57BL/6J	The Jackson Laboratory	Strain #: 000664
Atp4b^{Cre} [B6.FVB-Tg(Atp4b-cre)1Jig/JcmiJ]	The Jackson Laboratory	Strain #: 030656
Adar1^{fl}	Qingde Wang (University of Pittsburgh)	N/A
B6.Cg-Gt(ROSA)26Sor$^{tm9(CAG-tdTomato)Hze}$/J (Ai9 reporter)	The Jackson Laboratory	Strain #: 007909
Adar1$^{\Delta PC}$	Sáenz lab	N/A
Adar1$^{fl/fl}$;Atp4b^{Cre};Ai9		
Rag1$^{-/-}$[B6.129S7-Rag1^{tm1Mom}/J]	The Jackson Laboratory	Strain #: 002216
Ifnar1$^{-/-}$[B6(Cg)-Ifnar1$^{tm1.1Ees}$/J]	The Jackson Laboratory	Strain #: 028256
Ifnlr1$^{-/-}$	Megan Baldridge (Washington University in St. Louis School of Medicine)	N/A
Mavs$^{-/-}$[B6;129-Mavs^{tm1Zjc}/J]	The Jackson Laboratory	Strain #: 008634
Adar1$^{\Delta PC}$;Rag1$^{-/-}$	Sáenz lab	N/A
Adar1$^{\Delta PC}$;Ifnar1$^{-/-}$	Sáenz lab	N/A
Adar1$^{\Delta PC}$;Ifnlr1$^{-/-}$	Sáenz lab	N/A
Adar1$^{\Delta PC}$;Ifnar1$^{-/-}$; Ifnlr1$^{-/-}$	Sáenz lab	N/A
Adar1$^{\Delta PC}$;Mavs$^{-/-}$	Sáenz lab	N/A
Software and algorithms		Available upon request.
Deposited data		Available upon request.

with the following options: –min-alternate-count 2, –min-coverage 5, –min-base-quality 20, –min-mapping-quality 30, –min-supporting-mapping-qsum 30, –min-supporting-allele-qsum 20, –min-alternate-qsum 40, –use-mapping-quality.[64] We used SnpSift to extract positions with A-to-G and T-to-C modifications and annotated the modifications with snpEff to provide gene context. After annotating all edited sites, downstream analyses were performed in R. A threshold was set to filter for ADAR1-specific editing. Only sites edited at a frequency >5% in *Adar1*-sufficient parietal cells (WT) and reduced to <1% at that same site in *Adar1*-deficient parietal cells (KO) were selected as ADAR1-specific variants. Downstream analyses and plots were generated on the ADAR1-specific variants using ggplots.[65]

Statistical Analyses

Differences in group means were determined by the Student's *t*-test or by analysis of variance (ANOVA) and post-hoc Tukey tests for multiple comparisons, using GraphPad Prism 10. Differences were considered statistically significant for *P* values less than .05.

Supplementary Material

Note: To access the supplementary material accompanying this article, visit the full text version at https://doi.org/10.1016/j.jcmgh.2025.101673.

References

1. Sung H, Ferlay J, Siegel RL, et al. Global cancer statistics 2020: GLOBOCAN estimates of incidence and mortality worldwide for 36 cancers in 185 countries. CA Cancer J Clin 2021;71:209–249.
2. Ajani JA, Lee J, Sano T, et al. Gastric adenocarcinoma. Nat Rev Dis Primers 2017;3:17036.
3. Correa P, Piazuelo MB. The gastric precancerous cascade. J Dig Dis 2012;13:2–9.
4. Goldenring JR, Mills JC. Cellular plasticity, reprogramming, and regeneration: metaplasia in the stomach and beyond. Gastroenterology 2022;162:415–430.
5. Saenz JB, Vargas N, Cho CJ, Mills JC. Regulation of the double-stranded RNA response through ADAR1 licenses metaplastic reprogramming in gastric epithelium. JCI Insight 2022;7:e153511.
6. Takeuchi O, Akira S. Pattern recognition receptors and inflammation. Cell 2010;140:805–820.
7. Chan TH, Qamra A, Tan KT, et al. ADAR-mediated RNA editing predicts progression and prognosis of gastric cancer. Gastroenterology 2016;151:637–650.e10.
8. Liddicoat BJ, Piskol R, Chalk AM, et al. RNA editing by ADAR1 prevents MDA5 sensing of endogenous dsRNA as nonself. Science 2015;349:1115–1120.
9. Chen YG, Hur S. Cellular origins of dsRNA, their recognition and consequences. Nat Rev Mol Cell Biol 2022;23:286–301.
10. Mannion NM, Greenwood SM, Young R, et al. The RNA-editing enzyme ADAR1 controls innate immune responses to RNA. Cell Rep 2014;9:1482–1494.
11. Liddicoat BJ, Hartner JC, Piskol R, et al. Adenosine-to-inosine RNA editing by ADAR1 is essential for normal murine erythropoiesis. Exp Hematol 2016;44:947–963.
12. Shiromoto Y, Sakurai M, Minakuchi M, et al. ADAR1 RNA editing enzyme regulates R-loop formation and genome stability at telomeres in cancer cells. Nat Commun 2021;12:1654.
13. Jiang Q, Isquith J, Ladel L, et al. Inflammation-driven deaminase deregulation fuels human pre-leukemia stem cell evolution. Cell Rep 2021;34:108670.
14. Yan HHN, Siu HC, Law S, et al. A comprehensive human gastric cancer organoid biobank captures tumor subtype heterogeneity and enables therapeutic screening. Cell Stem Cell 2018;23:882–897.e11.
15. Wong TL, Loh JJ, Lu S, et al. ADAR1-mediated RNA editing of SCD1 drives drug resistance and self-renewal in gastric cancer. Nat Commun 2023;14:2861.
16. Dou N, Yu S, Ye X, et al. Aberrant overexpression of ADAR1 promotes gastric cancer progression by activating mTOR/p70S6K signaling. Oncotarget 2016;7:86161–86173.
17. Nam KT, Lee HJ, Sousa JF, et al. Mature chief cells are cryptic progenitors for metaplasia in the stomach. Gastroenterology 2010;139:2028–2037.e9.
18. Saenz JB, Mills JC. Acid and the basis for cellular plasticity and reprogramming in gastric repair and cancer. Nat Rev Gastroenterol Hepatol 2018;15:257–273.
19. Wang Q, Miyakoda M, Yang W, et al. Stress-induced apoptosis associated with null mutation of ADAR1 RNA editing deaminase gene. J Biol Chem 2004;279:4952–4961.
20. Kolberg L, Raudvere U, Kuzmin I, et al. g:Profiler-interoperable web service for functional enrichment analysis and gene identifier mapping (2023 update). Nucleic Acids Res 2023;51:W207–W212.
21. de Reuver R, Verdonck S, Dierick E, et al. ADAR1 prevents autoinflammation by suppressing spontaneous ZBP1 activation. Nature 2022;607:784–789.
22. Stetson DB, Medzhitov R. Type I interferons in host defense. Immunity 2006;25:373–381.
23. Mills KHG. IL-17 and IL-17-producing cells in protection versus pathology. Nat Rev Immunol 2023;23:38–54.
24. Belkaid Y, Hand TW. Role of the microbiota in immunity and inflammation. Cell 2014;157:121–141.
25. Mombaerts P, Iacomini J, Johnson RS, et al. RAG-1-deficient mice have no mature B and T lymphocytes. Cell 1992;68:869–877.
26. Goldenring JR, Nam KT. Oxyntic atrophy, metaplasia, and gastric cancer. Prog Mol Biol Transl Sci 2010;96:117–131.
27. Petersen CP, Mills JC, Goldenring JR. Murine models of gastric corpus preneoplasia. Cell Mol Gastroenterol Hepatol 2017;3:11–26.
28. O'Brien VP, Jackson LK, Frick JP, et al. Helicobacter pylori chronic infection selects for effective colonizers of metaplastic glands. mBio 2023;14:e0311622.
29. Nozaki K, Ogawa M, Williams JA, et al. A molecular signature of gastric metaplasia arising in response to acute parietal cell loss. Gastroenterology 2008;134:511–522.
30. Sun Q, Sun L, Liu HH, et al. The specific and essential role of MAVS in antiviral innate immune responses. Immunity 2006;24:633–642.

31. Zheng J, Shi W, Yang Z, et al. RIG-I-like receptors: Molecular mechanism of activation and signaling. Adv Immunol 2023;158:1–74.
32. Ablasser A, Hur S. Regulation of cGAS- and RLR-mediated immunity to nucleic acids. Nat Immunol 2020;21:17–29.
33. Odendall C, Dixit E, Stavru F, et al. Diverse intracellular pathogens activate type III interferon expression from peroxisomes. Nat Immunol 2014;15:717–726.
34. Chung H, Calis JJA, Wu X, et al. Human ADAR1 prevents endogenous RNA from triggering translational shutdown. Cell 2018;172:811–824.
35. Bockerstett KA, Lewis SA, Noto CN, et al. Single-cell transcriptional analyses identify lineage-specific epithelial responses to inflammation and metaplastic development in the gastric corpus. Gastroenterology 2020; 159:2116–2129.e4.
36. Bockerstett KA, Lewis SA, Wolf KJ, et al. Single-cell transcriptional analyses of spasmolytic polypeptide-expressing metaplasia arising from acute drug injury and chronic inflammation in the stomach. Gut 2020; 69:1027–1038.
37. Adkins-Threats M, Mills JC. Cell plasticity in regeneration in the stomach and beyond. Curr Opin Genet Dev 2022;75:101948.
38. Engevik AC, Kaji I, Goldenring JR. The physiology of the gastric parietal cell. Physiol Rev 2020;100:573–602.
39. Fumagalli D, Gacquer D, Rothe F, et al. Principles governing A-to-I RNA editing in the breast cancer transcriptome. Cell Rep 2015;13:277–289.
40. Riera KM, Jang B, Min J, et al. Trop2 is upregulated in the transition to dysplasia in the metaplastic gastric mucosa. J Pathol 2020;251:336–347.
41. Huh WJ, Khurana SS, Geahlen JH, et al. Tamoxifen induces rapid, reversible atrophy, and metaplasia in mouse stomach. Gastroenterology 2012;142:21–24.e7.
42. Saenz JB, Vargas N, Mills JC. Tropism for spasmolytic polypeptide-expressing metaplasia allows Helicobacter pylori to expand its intragastric niche. Gastroenterology 2019;156:160–174.e7.
43. Burclaff J, Osaki LH, Liu D, et al. Targeted apoptosis of parietal cells is insufficient to induce metaplasia in stomach. Gastroenterology 2017;152:762–766.e7.
44. Mittal P, Roberts CWM. The SWI/SNF complex in cancer - biology, biomarkers and therapy. Nat Rev Clin Oncol 2020;17:435–448.
45. Silver RF, Xia M, Storer CE, et al. Distinct gene expression signatures comparing latent tuberculosis infection with different routes of Bacillus Calmette-Guerin vaccination. Nat Commun 2023;14:8507.
46. Gyorffy B. Integrated analysis of public datasets for the discovery and validation of survival-associated genes in solid tumors. Innovation (Camb) 2024;5:100625.
47. Cancer Genome Atlas Research Network. Comprehensive molecular characterization of gastric adenocarcinoma. Nature 2014;513:202–209.
48. Lee S, Baldridge MT. Interferon-lambda: a potent regulator of intestinal viral infections. Front Immunol 2017;8:749.
49. de Weerd NA, Vivian JP, Nguyen TK, et al. Structural basis of a unique interferon-beta signaling axis mediated via the receptor IFNAR1. Nat Immunol 2013; 14:901–907.
50. Lazear HM, Nice TJ, Diamond MS. Interferon-lambda: immune functions at barrier surfaces and beyond. Immunity 2015;43:15–28.
51. Dhir A, Dhir S, Borowski LS, et al. Mitochondrial double-stranded RNA triggers antiviral signalling in humans. Nature 2018;560:238–242.
52. Karki R, Sundaram B, Sharma BR, et al. ADAR1 restricts ZBP1-mediated immune response and PANoptosis to promote tumorigenesis. Cell Rep 2021;37:109858.
53. Zhang T, Yin C, Fedorov A, et al. ADAR1 masks the cancer immunotherapeutic promise of ZBP1-driven necroptosis. Nature 2022;606:594–602.
54. Han L, Diao L, Yu S, et al. The genomic landscape and clinical relevance of A-to-I RNA editing in human cancers. Cancer Cell 2015;28:515–528.
55. Paz-Yaacov N, Bazak L, Buchumenski I, et al. Elevated RNA editing activity is a major contributor to transcriptomic diversity in tumors. Cell Rep 2015;13:267–276.
56. Dobin A, Davis CA, Schlesinger F, et al. STAR: ultrafast universal RNA-seq aligner. Bioinformatics 2013;29:15–21.
57. Liao Y, Smyth GK, Shi W. featureCounts: an efficient general purpose program for assigning sequence reads to genomic features. Bioinformatics 2014;30:923–930.
58. Patro R, Duggal G, Love MI, et al. Salmon provides fast and bias-aware quantification of transcript expression. Nat Methods 2017;14:417–419.
59. Robinson MD, McCarthy DJ, Smyth GK. edgeR: a Bioconductor package for differential expression analysis of digital gene expression data. Bioinformatics 2010; 26:139–140.
60. Ritchie ME, Phipson B, Wu D, et al. limma powers differential expression analyses for RNA-sequencing and microarray studies. Nucleic Acids Res 2015;43:e47.
61. Liu R, Holik AZ, Su S, et al. Why weight? Modelling sample and observational level variability improves power in RNA-seq analyses. Nucleic Acids Res 2015;43:e97.
62. Hoft SG, Brennan M, Carrero JA, et al. Unveiling cancer-related metaplastic cells in both Helicobacter pylori infection and autoimmune gastritis. Gastroenterology 2025;168:53–67.
63. Gao Y, Chen S, Halene S, Tebaldi T. Transcriptome-wide quantification of double-stranded RNAs in live mouse tissues by dsRIP-Seq. STAR Protoc 2021;2:100366.
64. Garrison E, Marth G. Haplotype-based variant detection from short-read sequencing; 2012, arXiv:1207.3907.
65. Wickham H. ggplot2 : Elegant graphics for data analysis. 2nd ed. Cham: Springer International Publishing, 2016, 1 online resource.

Received June 18, 2025. Accepted October 29, 2025.

Correspondence
Address correspondence to: José B. Sáenz, MD, PhD, Division of Gastroenterology, Department of Medicine, Department of Molecular Cell Biology, 660 S. Euclid Avenue, Campus Box 8124, St Louis, Missouri 63110; tel: (314) 273-4762. e-mail: saenzj@wustl.edu.

Acknowledgments
The authors thank Eric Tycksen (Genome Technology Access Center, Washington University in St. Louis School of Medicine) for assistance with RNA-seq analysis.

CRediT Authorship Contributions
Angela Halstead, PhD (Conceptualization: Equal; Data curation: Equal; Formal analysis: Equal; Investigation: Equal; Methodology: Lead; Project administration: Lead; Validation: Equal; Writing – review & editing: Equal)

Chinye Nwokolo, BS (Data curation: Supporting; Formal analysis: Supporting; Software: Equal; Validation: Equal; Writing – review & editing: Supporting)

Stella Hoft, BA (Formal analysis: Equal; Investigation: Equal; Writing – review & editing: Supporting)

Jinsheng Yu, PhD (Data curation: Equal; Formal analysis: Equal; Software: Equal; Validation: Equal; Writing – review & editing: Supporting)

Lifei Zhu, MD, PhD (Formal analysis: Supporting; Methodology: Supporting)

Brendan Tuley, BS (Formal analysis: Supporting; Investigation: Supporting; Methodology: Supporting)

Nancy Vargas, PhD (Investigation: Supporting; Methodology: Supporting)

RuiRui Liu, BS (Formal analysis: Supporting; Investigation: Supporting)

Francisco Victorino, PhD (Formal analysis: Supporting; Investigation: Equal; Methodology: Supporting; Writing – review & editing: Supporting)

Simrin Phatak, BS (Formal analysis: Supporting)

Wandy Beatty, PhD (Formal analysis: Supporting; Methodology: Supporting)

Chun-Kan Chen, PhD (Formal analysis: Equal; Software: Supporting; Writing – original draft: Supporting)

Richard DiPaolo, PhD (Conceptualization: Supporting; Resources: Supporting; Writing – review & editing: Supporting)

Paul Cliften, PhD (Formal analysis: Supporting; Methodology: Supporting; Software: Supporting; Writing – review & editing: Supporting)

Tarin M. Bigley, MD, PhD (Conceptualization: Supporting; Formal analysis: Supporting; Investigation: Supporting; Methodology: Supporting; Resources: Supporting; Writing – review & editing: Supporting)

Jose Bernardo Saenz, MD, PhD (Conceptualization: Lead; Data curation: Equal; Formal analysis: Equal; Funding acquisition: Lead; Investigation: Equal; Methodology: Equal; Project administration: Equal; Resources: Equal; Supervision: Lead; Validation: Lead; Visualization: Lead; Writing – original draft: Lead; Writing – review & editing: Lead)

Conflicts of interest
The authors disclose no conflicts.

Funding
Research reported in this publication was supported by the National Institute of Diabetes and Digestive and Kidney Diseases of the National Institutes of Health under Award Numbers K08DK122116, R03DK133423, and R01DK141682 (José Bernardo Saenz); Digestive Diseases Research Core Center (Washington University in St Louis School of Medicine; José Bernardo Saenz), and the Gastric Cancer Research Innovation Fund (The Foundation for Barnes-Jewish Hospital; José Bernardo Saenz).

Data Availability
Data, analytic methods, and study material will be made directly available, upon request.